February 1989 ANL-IFR-104

COMPATIBILITY OF LOW-BURNUP U-10Zr FUEL WITH HT9 CLADDING AT ELEVATED TEMPERATURES

by

H. Tsai, F. E. Savoie, L. R. Kelman, and W. D. Jackson

Materials and Components Technology Division
Argonne National Laboratory
9700 South Cass Avenue
Argonne, Illinois 60439

IFR TECHNICAL MEMORANDUM NO. 104

~~Results reported in~~ the IFR-TM series of memoranda ~~frequently are preliminary and subject to revision. Consequently they should not be quoted or referenced.~~

DISCLAIMER

TABLE OF CONTENTS

LIST OF FIGURES

LIST OF FIGURES (Contd.)

LIST OF TABLES

COMPATIBILITY OF LOW-BURNUP U-10Zr FUEL WITH HT9 CLADDING AT ELEVATED TEMPERATURES

by

H. Tsai, F. E. Savoie, L. R. Kelman, and W. D. Jackson

ABSTRACT

A series of fuel-cladding compatibility tests was conducted on low-burnup (~2.9 a/o) U-10Zr fuel with HT9 cladding in the temperature range between 700 and 850°C. Following the tests, the specimens were metallographically examined to determine the condition of the fuel and cladding and to measure the maximum cladding wastage. One of the specimens was examined with the scanning electron microscope to identify the phases and constituents involved in the fuel-cladding metallurgical interaction.

The results of these tests showed the fuel-cladding interaction to be a liquid-phase attack of the cladding. Onset of interaction occurred at a temperature between 700 and 750°C. When interaction occurred, Fe and Cr, the major constituents of the HT9 cladding, migrated into the fuel, resulting in the lowering of the fuel solidus temperature. At the same time, a significant amount of reaction between the fuel and cladding constituents took place at the fuel-cladding interface. The reaction boundary in the cladding was found to be sharply defined. There was no intergranular or intragranular penetration or cracking in the unreacted cladding, which was found to be ductile and capable of arresting crack propagation. The measured maximum rate of cladding penetration agreed well with the current ANL correlation.

I. INTRODUCTION

Compatibility between metallic IFR fuels and cladding at elevated temperatures is important because it impacts the performance of the fuel system during off-normal reactor events. A principal objective of the IFR fuel-cladding compatibility tests is to define a correlation describing the rates of cladding penetration (wastage) as functions of temperature and other applicable parameters, thus providing a means to evaluate the integral fuel pin performance, including pin lifetime, for perceived off-normal reactor events.

A series of seven compatibility tests on fuel pin segments of irradiated U-10Zr fuel with HT9 cladding was conducted in the Fuel Behavior Test Apparatus (FBTA) located at the Alpha-Gamma Hot Cell Facility (AGHCF). The U-10Zr fuel with HT9 cladding is the current candidate for both the EBR-II Mk-IV and FFTF Series-III driver fuel systems. The results of these tests are the subject of this report.

II. EXPERIMENTAL TECHNIQUE

A. Specimen Preparation

The test specimens, ~8-mm (0.3-in)-long segments of irradiated fuel with cladding, were taken from pin T437 of EBR-II S/A X425 at ~2.9 a/o peak burnup.[1] The fuel material was U-10w/oZr with a beginning-of-life (BOL) planar smear density of 75% TD. The cladding was tempered martensitic HT9 with an OD of 5.84 mm (0.230 in.) and a wall thickness of 0.38 mm (0.015 in.). Three specimens were from near the top of the fuel column (x/ℓ = 0.84 to 0.90) and the others were from near the midplane (x/ℓ = 0.42 to 0.52). The principal difference between these two groups of specimens was the condition of the fuel-cladding gap, which was open in the specimens from near the top and closed in those from near the midplane. The open fuel-cladding gap near the top was due to the lower fuel swelling at this location and burnup level. Before the tests, the ends of the specimens were ground square and

photographed. Each specimen was weighed to determine whether the inside of the specimen contained excessive porosity not detectable from the end views.

The specimens were prepared in the high-purity nitrogen cell at the AGHCF, where the oxygen content was typically maintained at <~250 ppm. After cutting and grinding, the specimens were kept in small sealed vials to minimize oxidation until testing.

B. Fuel Behavior Test Apparatus

The compatibility tests discussed in this report were conducted in the FBTA, which consists of an axisymmetric infrared radiant furnace to provide specimen heating, a helium-gas purge system to provide an inert atmosphere and to remove the released fission gas from the test specimen, a thermocouple to measure the specimen temperature, an LVDT (linear variable differential transformer) system to measure the specimen height, and a microcomputer system to perform furnace control, trip protection and data acquisition functions. A prior version of the FBTA (designated DEH, for direct electric heating) was used in the measuring of fission gas retention and axial expansion of irradiated IFR metallic fuels.[2,3]

In the FBTA, the specimen was placed in a tantalum cup in an upright position at the center of the heating zone. The test temperature was measured with an unsheathed Pt/Pt-10Rh (Type S) thermocouple welded onto the outside of the tantalum cup. A new cup/thermocouple assembly was used in each test. A hold-down rod, connected to the LVDT, was placed over the top of the specimen to monitor the collapsing of a specimen should gross fuel melting occur. The physical isolation between the furnace heating elements and the test specimen was provided by two concentric quartz tubes. A helium gas flow in the inner quartz tubing provided an inert environment for the specimen during the test and prevented the released volatile fission products from coating the quartz tube. A schematic diagram showing the specimen and the radiant furnace is given in Fig. 1. A photograph of the furnace and specimen assembly is shown in Fig. 2.

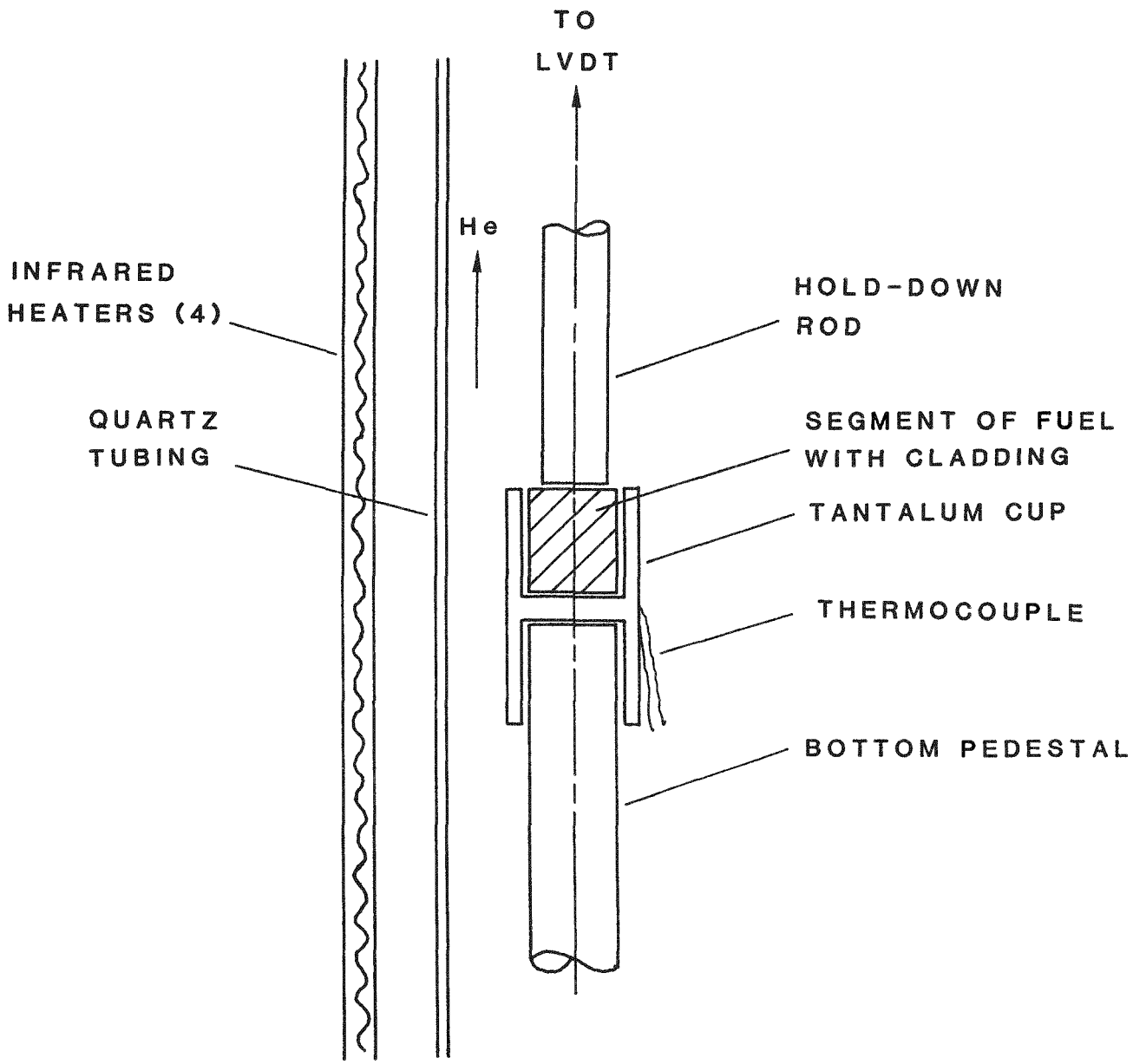

Fig. 1. Schematic Diagram of the Fuel Behavior Test Apparatus.

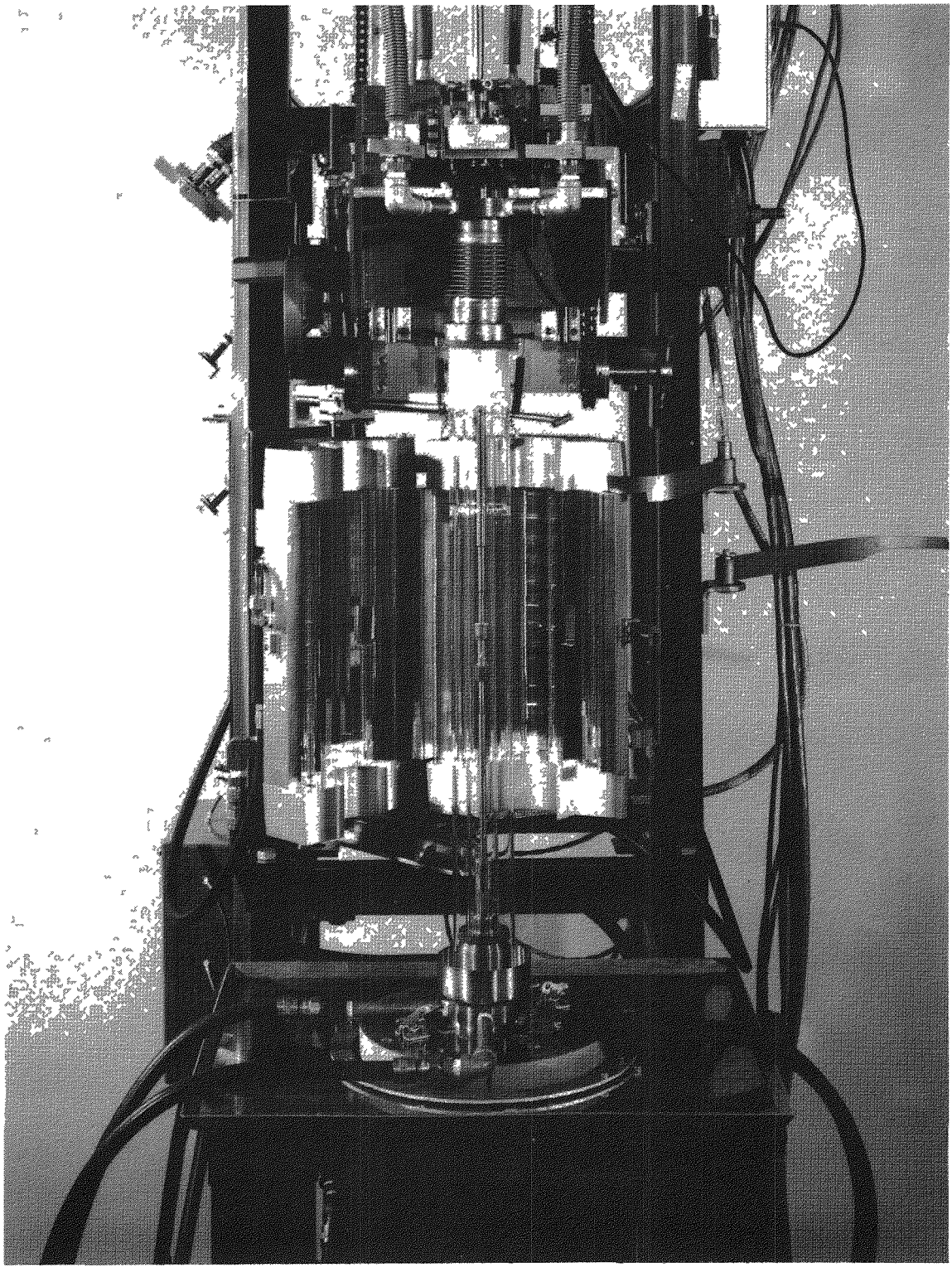

Fig. 2. The Fuel Behavior Test Apparatus (FBTA), Shown With the Furnace Half-Shell Open. (ANL Neg. No. 306-81-18K)

The thermoelectric voltage output from the Type S specimen thermocouple was connected to a digital thermometer. The analog output from the digital thermometer was directed to the microcomputer for furnace power control and temperature recording. The accuracy of the thermocouples used in these tests was certified by the vendor to be within ±2°C below 800°C (ANSI Standard MC 96.1). The digital thermometer was verified against NBS-calibrated equipment to be within ±1°C of the Type S thermocouple standard in the test temperature range. The entire temperature measurement system was further validated against the melting temperature of NBS-supplied pure aluminum (660.3°C m.p.) and found to be within ±4°C.

To provide a rapid rate of temperature ascent during start-up and to maintain a constant test temperature, a microcomputer system was employed. The system compared the measured specimen temperature with the preset test temperature and adjusted the power input to the radiant furnace. The selected feedback constants for the control system produced the following desirable features: (1) reaching the test temperature in, typically, 50 s or less; (2) having a temperature overshoot of no more than ~12°C at the end of the temperature ascent; and (3) maintaining a constant temperature within ~2°C during the steady-state portion of the test. The recorded temperature history of a typical test is shown in Fig. 3. In addition to providing furnace power control, the microcomputer is capable of generating trip signals to scram the furnace when abnormal conditions, such as a temperature excursion or a flow reduction, occur.

Figure 4 shows a photograph of the FBTA control console and the furnace during operation.

C. Test Procedures

After the specimen was loaded in the FBTA, the helium purge flow was turned on for several minutes before the furnace was powered up. The hold time for each test at the desired test temperature was one hour. At the end of the test period, the system was scrammed and the specimen allowed to cool by radiant and convective heat losses. Cooldown to below 500°C typically took less than 30 s after the scram.

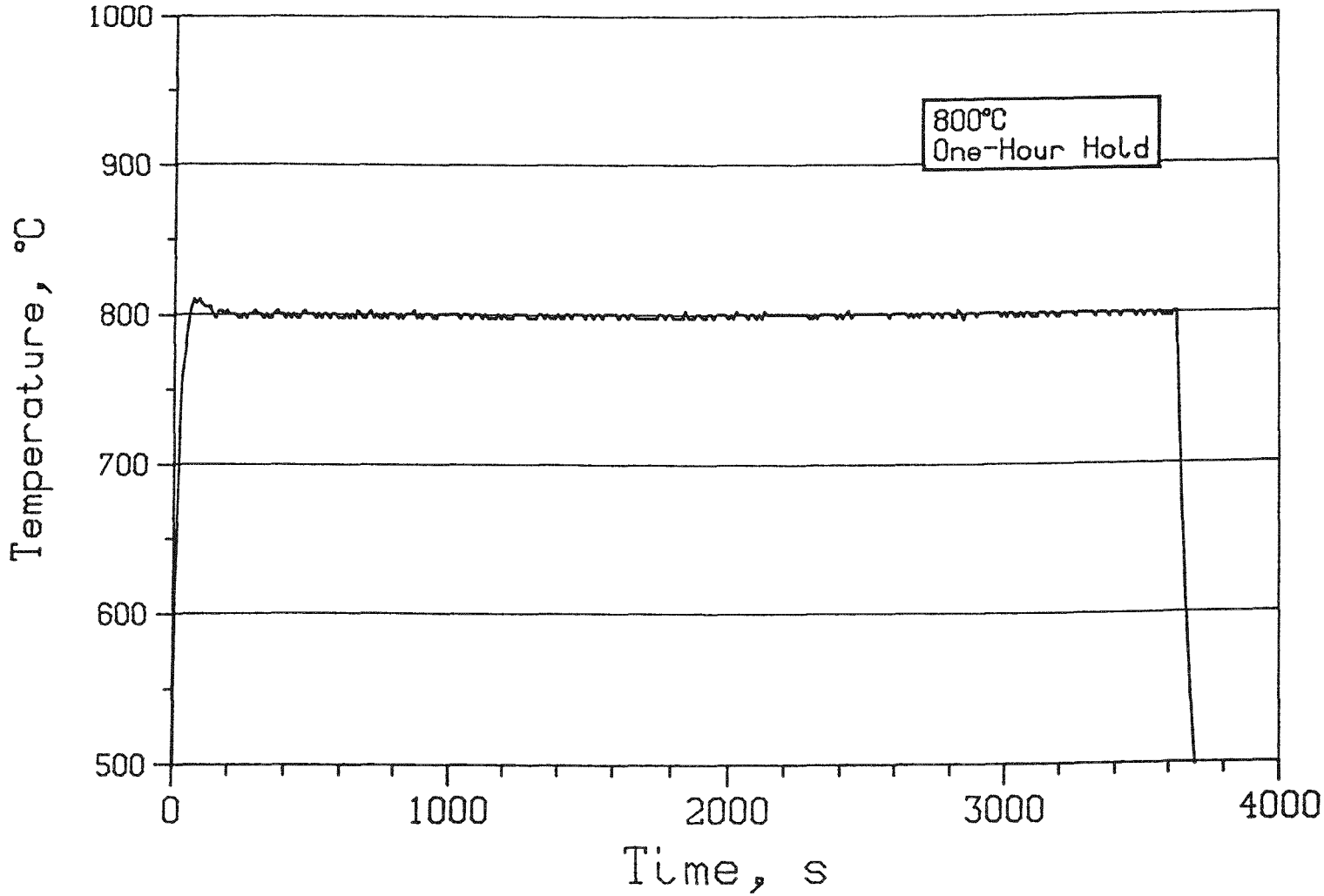

Fig. 3. Temperature History of FBTA Test 88-04.

FURNACE

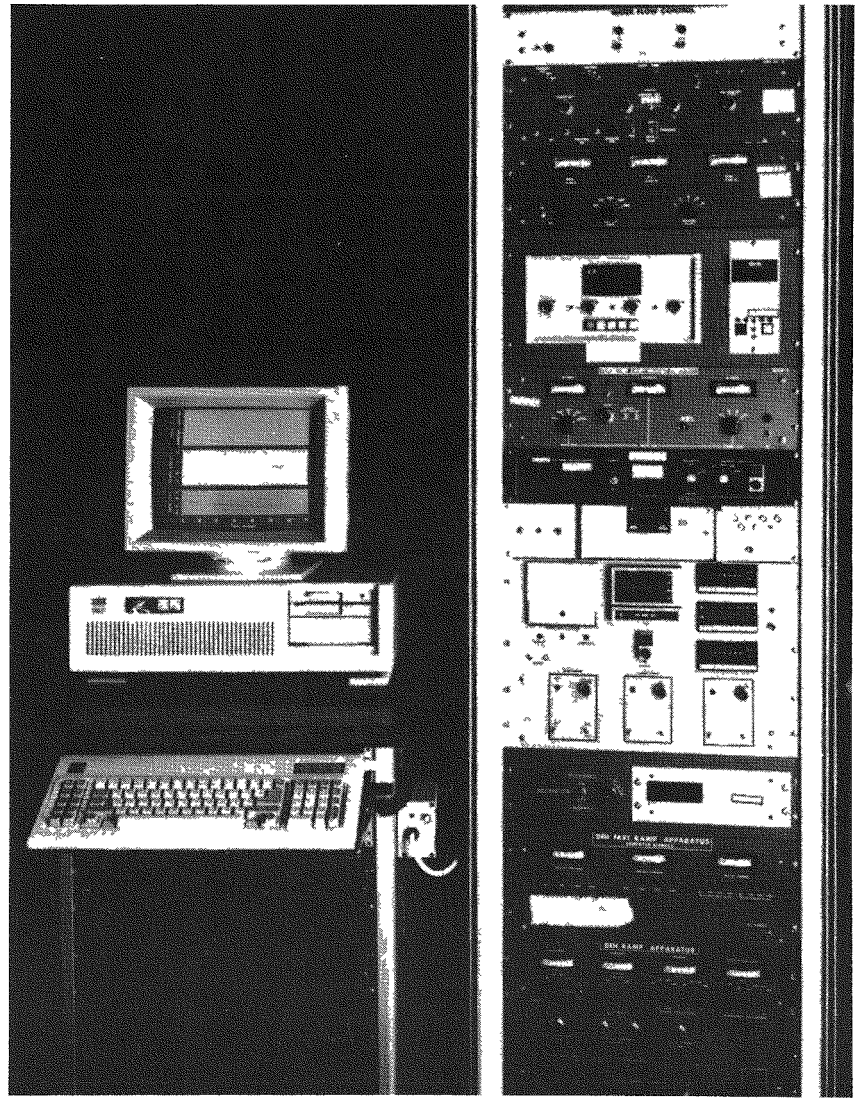

FBTA CONTROL CONSOLE

Fig. 4. The In-Cell Furnace and the FBTA Control Console.

Following the tests, the specimens were metallographically examined at the AGHCF. A polished, transverse section at ~1.5 mm below the top surface was prepared for the examination. In all cases, the boundary of cladding penetration was clearly identifiable with the specimen in the as-polished condition. From the ~150-200X photocomposites of the cladding, the thickness of the thinnest portion of the unreacted cladding was measured. The maximum cladding penetration was calculated as the difference between the original cladding thickness and the thinnest unreacted cladding. As the measurement accuracy of thickness on the 150-200X photograph was ~0.5 mm, the accuracy of the depth of penetration determination was 0.5 mm/150X, or ~0.003 mm. In terms of penetration rate, the accuracy was ~1 x 10^{-3} μm/s.

One of the 800°C test specimens was examined by scanning electron microscopy (SEM) and energy-dispersive X-ray analysis (EDX) to determine the phases formed in the reacted fuel and cladding. The SEM samples were prepared by cutting a thin transverse slice, ~0.25 mm (0.010 in.) thick, of the fuel and cladding from the middle portion of the specimen with a radial cutoff saw. During the postcutting operation, the thin fuel disk and the cladding ring were found to have separated, apparently owing to the weak bonding between the two. A piece of the fuel from near the fuel surface and a section of the cladding were separately mounted for the SEM examination.

III. TEST MATRIX

Seven tests, designated 88-01 through 88-06 and 88-10, are included in this report. The key parameters of the tests are summarized in Table I.

IV. TEST RESULTS

A. Results of Optical Metallographic Examination

At 700°C, no fuel-cladding interaction was noted after one hour. The transverse section of the 700°C (FBTA test 88-06) specimen under the optical microscope is shown in Fig. 5. The condition of the specimen is essentially the same as that of the as-irradiated steady-state sibling.[1]

TABLE I. Key Parameters of the Compatibility Tests[a]

FBTA Test No.	Specimen Axial Location (x/ℓ)	Fuel-Cladding Gap Condition	Test Temperature (°C)
88-06	0.49	Closed	700
88-05	0.45	Closed	750
88-04	0.43	Closed	800
88-10	0.51	Closed	800
88-03	0.89	Open	750
88-01	0.85	Open	800
88-02	0.87	Open	850

[a]All specimens were obtained from EBR-II Pin T437, S/A X425, at ~2.9 a/o peak burnup. The fuel material was U-10w/oZr and the cladding was HT9. The hold time at the test temperature was one hour in all cases.

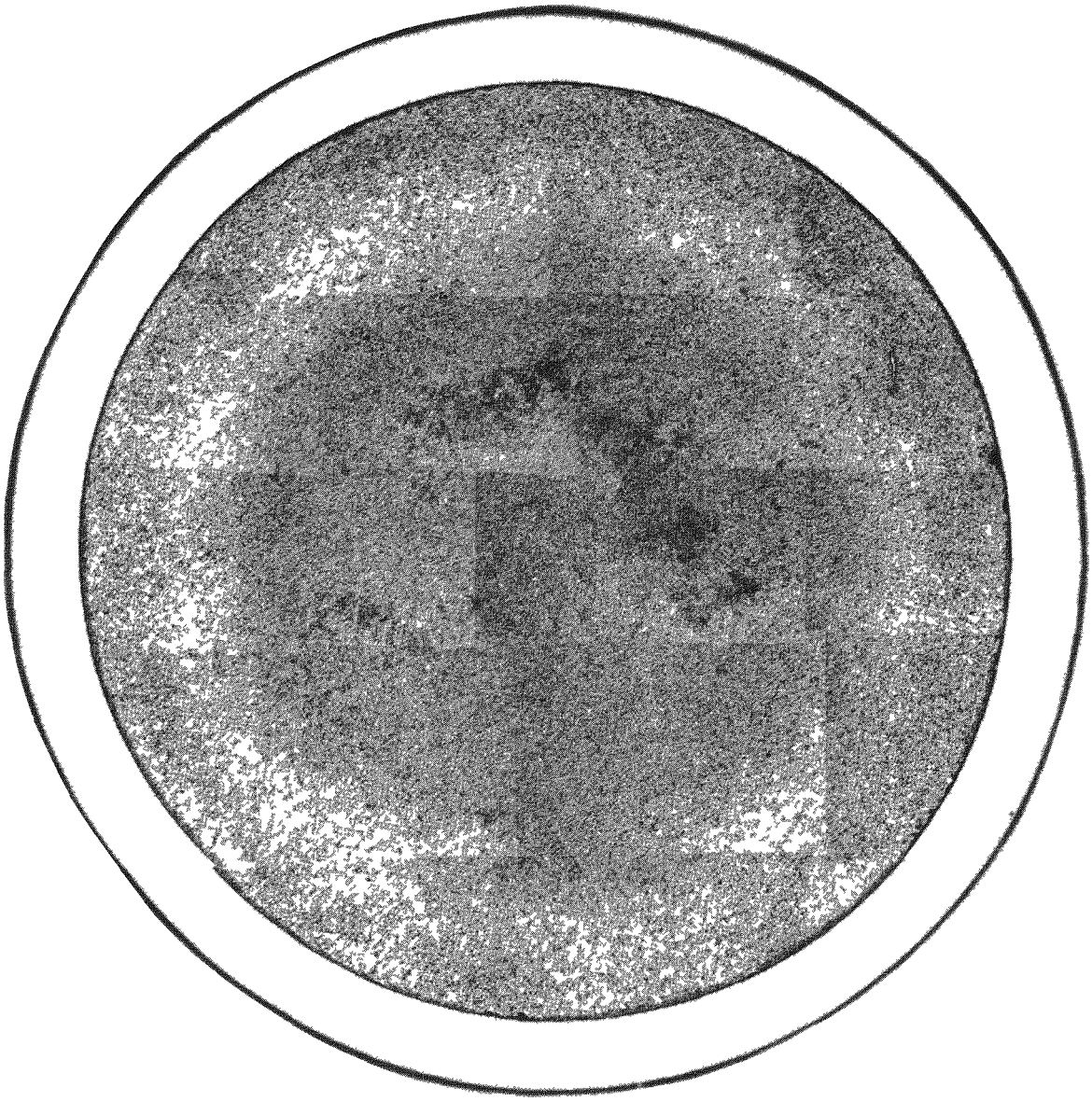

Fig. 5. As-polished Transverse Section of the U-10Zr/HT9 Specimen After Test 88-06 at 700°C for 1 Hour. (26X, MCT 244143)

At test temperatures of 750°C and higher, fuel-cladding interaction resulting in the formation of liquid phases could be noted. This is illustrated in Figs. 6 and 7 for the 750 and 800°C test specimens, respectively.

In the 750°C specimen (FBTA 88-05), nearly uniform fuel-cladding interaction, to a depth of ~10% of the fuel radius, occurred over ~80% of the fuel circumference. Large pores formed in the once-molten fuel zone, indicating the mobility of the liquid phase under the influence of the released fission gas.

In the 800°C test specimen (FBTA 88-04), owing to the higher test temperature, the reaction was substantially more extensive. Only the central zone from approximately mid-radius retained the original as-irradiated fuel microstructure. The reaction in the fuel in the circumferential direction was quite uniform. Large voids in the reacted fuel were created by the expulsion of the liquid phases through the open ends of the specimen.

The condition of the reacted cladding of the 800°C specimen is shown in Fig. 8. The boundary separating the reacted and the unaffected cladding appeared to be smooth and well defined. There were no intergranular or intragranular cladding cracks ahead of the visible reaction boundary. On the optical photomicrographs, at least two reaction zones in the cladding could be noted, with the outer zone having a structure that consisted of radially oriented phases. There were numerous circumferential cracks between the reacted fuel and reacted cladding. These cracks probably developed during the shutdown as a result of the differential thermal contraction.

Figure 9 shows an azimuthal section of the 800°C specimen cladding where only limited cladding reaction occurred. The lack of cladding reaction may be attributed to the presence of the thick surface layer on the fuel, which might have acted as a protective barrier for the cladding.

The test specimens for three of the tests in this series, 88-01, 88-02, and 88-03, were from near the top of the fuel column and had open fuel-cladding gaps. (All other specimens were from near the midplane and had

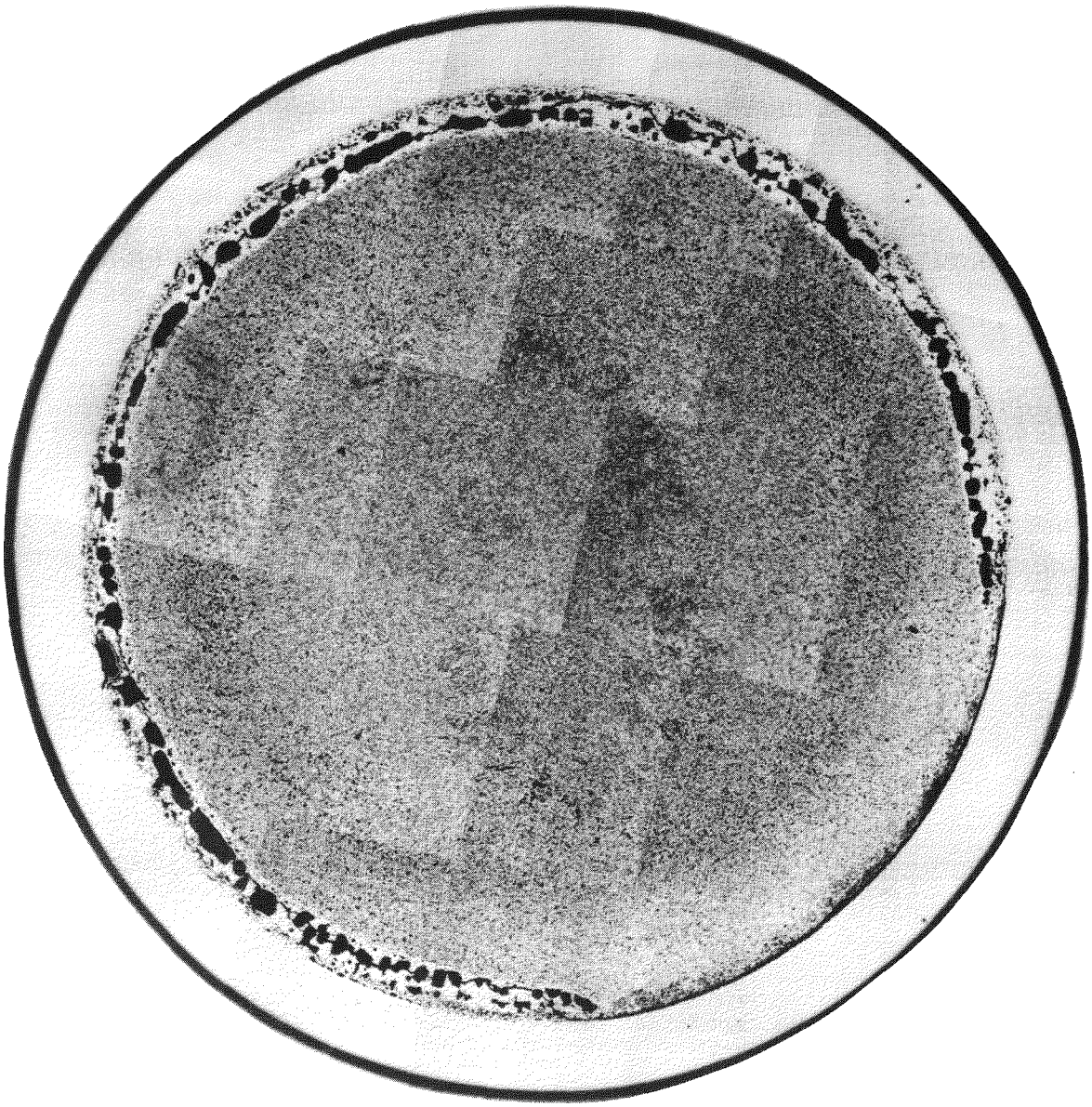

Fig. 6. As-polished Transverse Section of the U-10Zr/HT9 Specimen After Test 88-05 at 750°C for 1 Hour. (26X, MCT 244140)

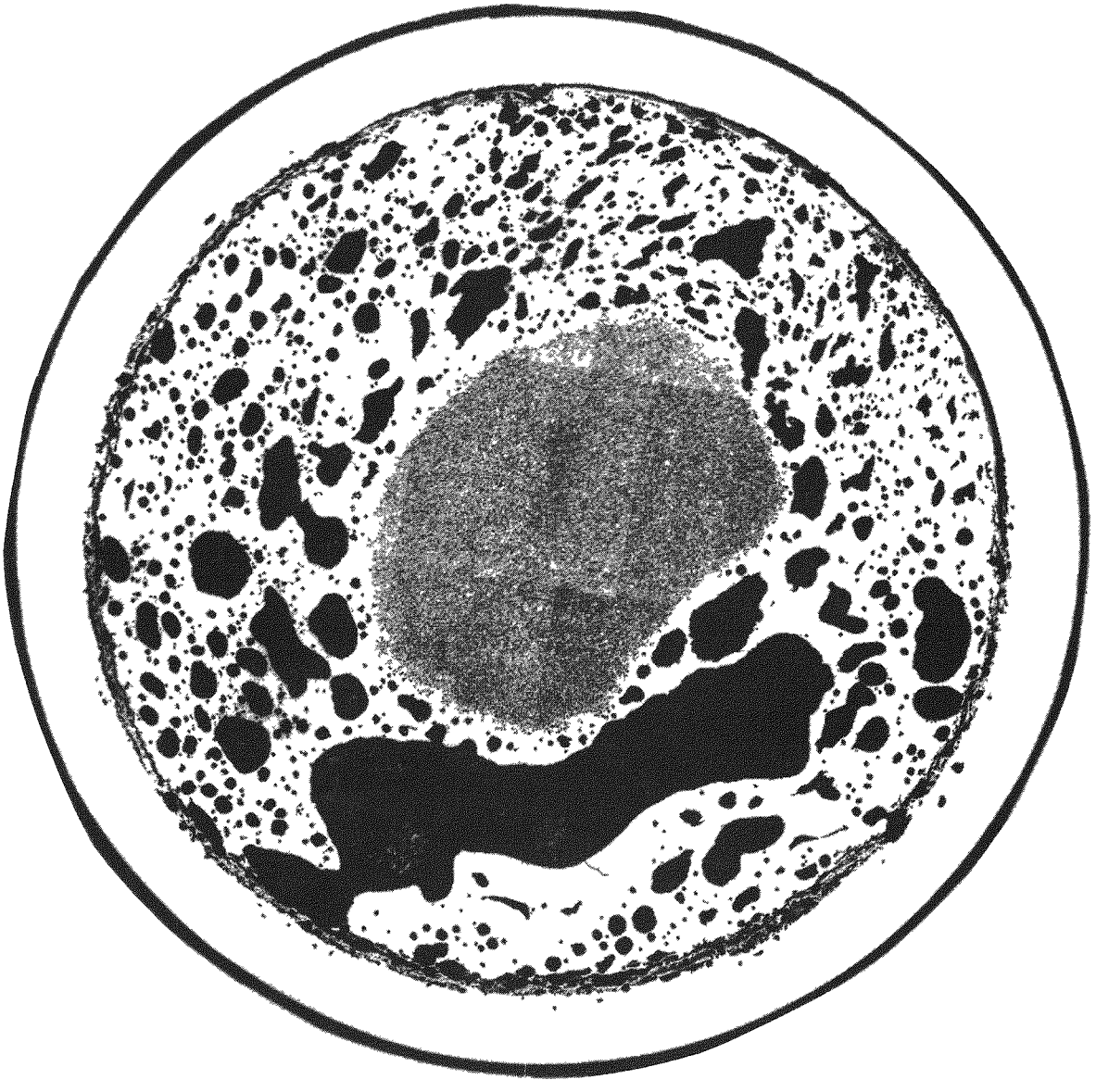

Fig. 7. As-polished Transverse Section of the U-10Zr/HT9 Specimen After Test 88-04 at 800°C for 1 Hour. (26X, MCT 244038)

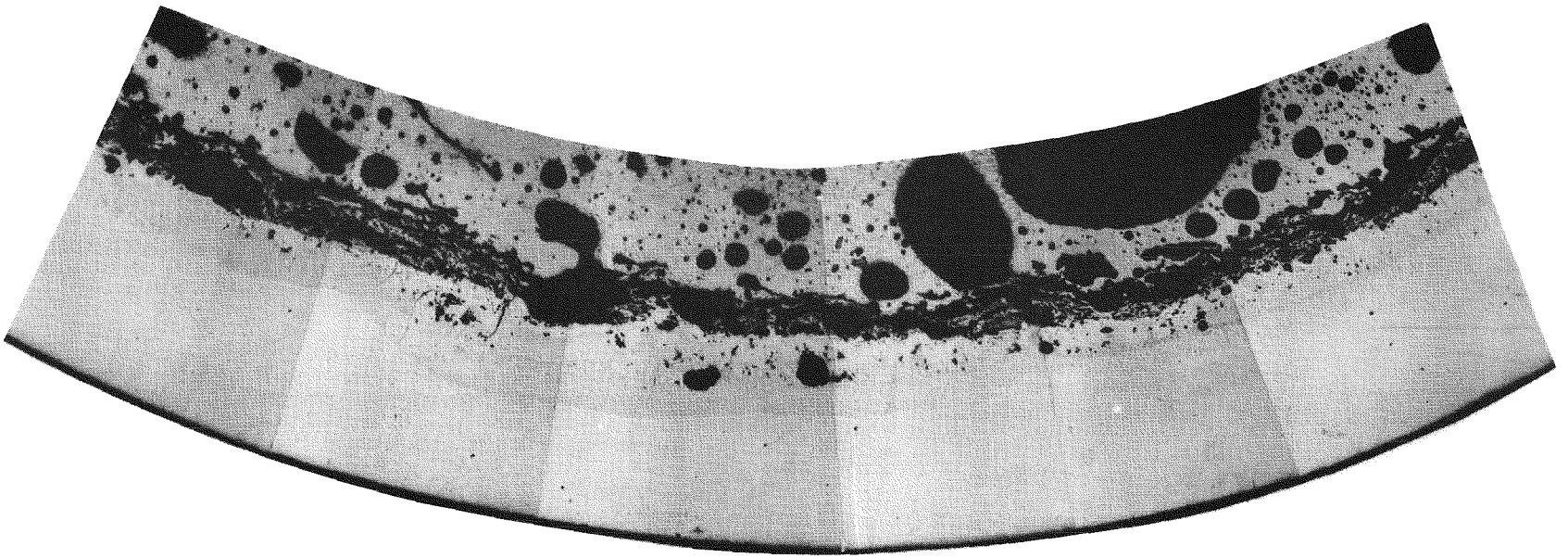

Fig. 8. Condition of the Reacted Cladding in the 88-04 Specimen. (77X, AP, MCT 244040)

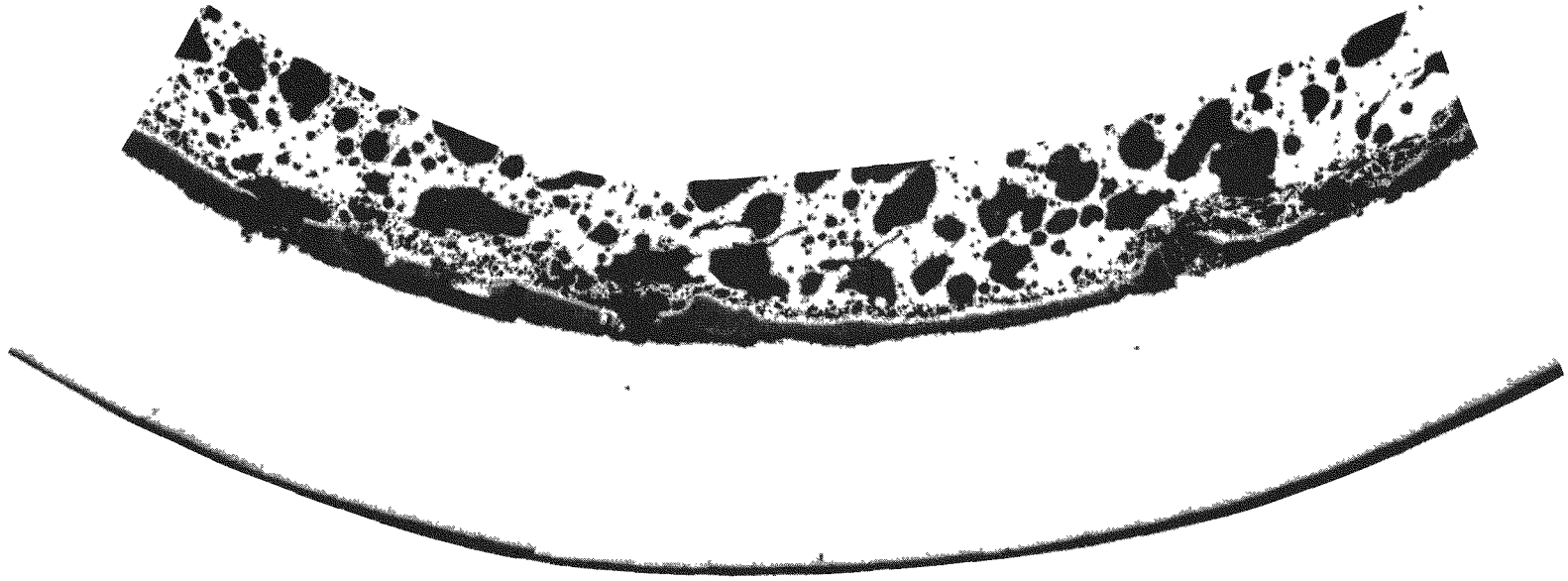

Fig. 9. Lack of Cladding Penetration in This Region of the 88-04 Specimen May Be Attributed to the Presence of the Thick Layer(s) on the Fuel Outer Surface. (77X, AP, MCT 244039)

closed fuel-cladding gaps.) The extent of fuel-cladding interaction in these specimens was substantially less than in those with the closed gaps at the same test temperatures. Comparison of open- and closed-gap specimens are shown in Figs. 10 (750°C tests) and 11 (800°C tests). At these two temperatures, the open-gap specimens actually showed no discernible cladding interaction. Substantial interaction, however, was noted on one side of the open-gap specimen tested at 850°C (FBTA 88-02). A transverse section of this specimen is shown in Fig. 12.

A comparison of the microstructure of the reacted fuel and the unreacted fuel in the 88-02 specimen is shown in Fig. 13. The once-molten reacted fuel had a two-phase structure consisting of a light acicular phase in a darker matrix phase. This two-phase structure was studied in detail by SEM/EDX, as will be reported later. Owing to the melting, many of the small fission gas bubbles coalesced and some undoubtedly vented from the ends of the specimen. Figure 14 shows the azimuthal section of the fuel-cladding interface where maximum cladding penetration occurred in the 88-02 specimen. Numerous hairline cracks, in a generally radial direction, were found in the reaction zone in the cladding. The presence of these cracks suggests that the solidified reacted cladding is brittle and would be unable to bear loads. However, all of the cracks terminated before reaching the unreacted cladding, indicating the unreacted cladding was still ductile and was not degraded. The results of the microhardness measurements conducted on the specimen, shown in Fig. 15, confirmed these observations. The hardness of the cladding away from the reaction zone was ~260 DPH, approximately the same as that of the unirradiated cladding. Immediately outside of the reaction zone, the hardness dropped to ~190 DPH, possibly reflecting a local depletion of carbon. In the reacted zone, the measured hardness was very high, in excess of 600 DPH.

B. Depths and Rates of Cladding Penetration

From the metallographic examination data, the maximum depths of cladding penetration of every specimen except specimen 88-10, which was only examined

Open–gap Specimen
(FBTA 88–03)

Closed–gap Specimen
(FBTA 88–05)

Fig. 10. Comparison of the Open- and Closed-Gap Specimens after 750°C Tests. (16.8X, MCT 246169)

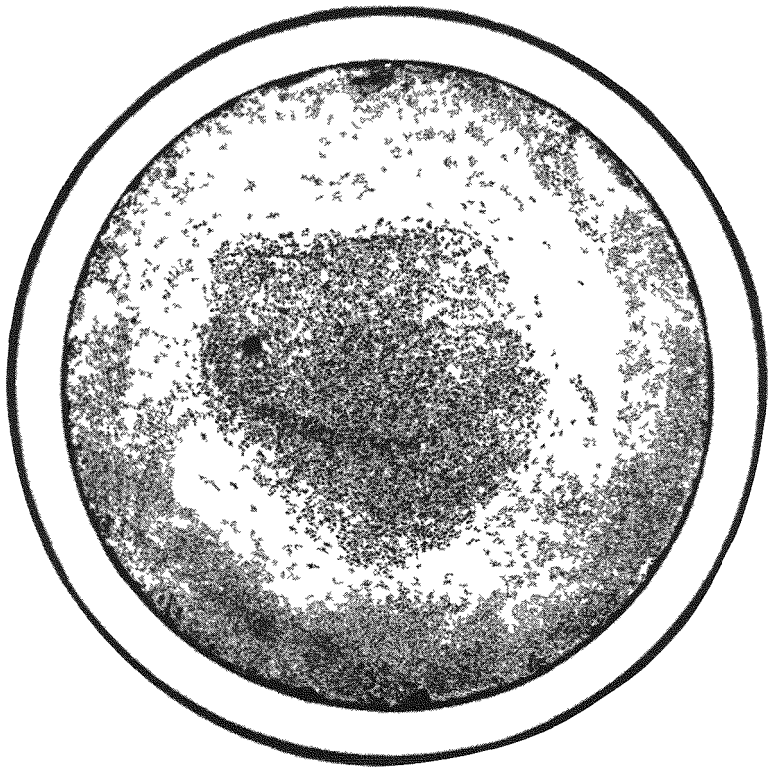

Open–gap Specimen
(FBTA 88–01)

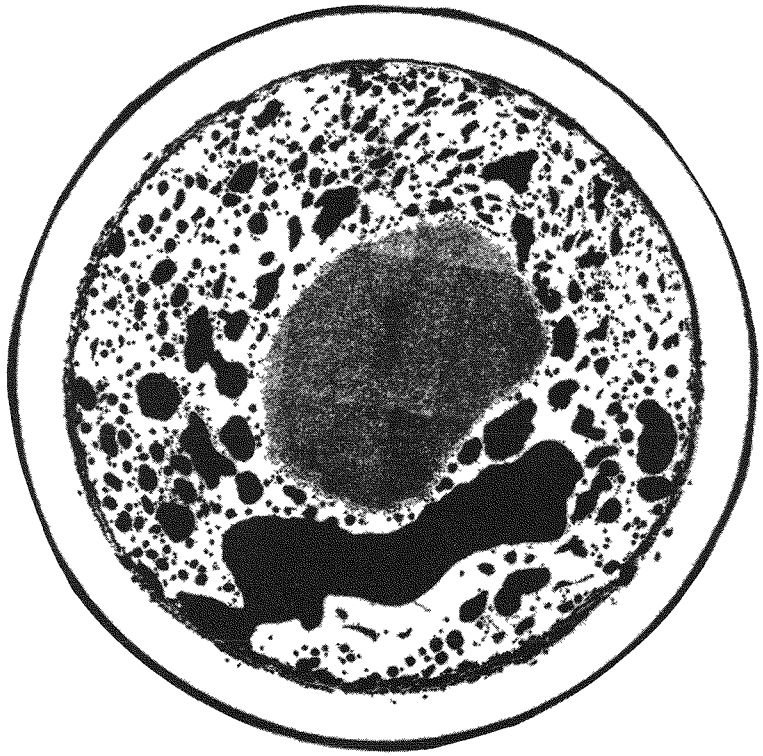

Closed–gap Specimen
(FBTA 88–04)

Fig. 11. Comparison of the Open- and Closed-Gap Specimens after 800°C Tests. (16.8X, MCT 246168)

Fig. 12. As-polished Transverse Section of the Open-Gap U-10Zr/HT9 Specimen after the 88-02 Test at 850°C for 1 Hour. (26X, MCT 243910)

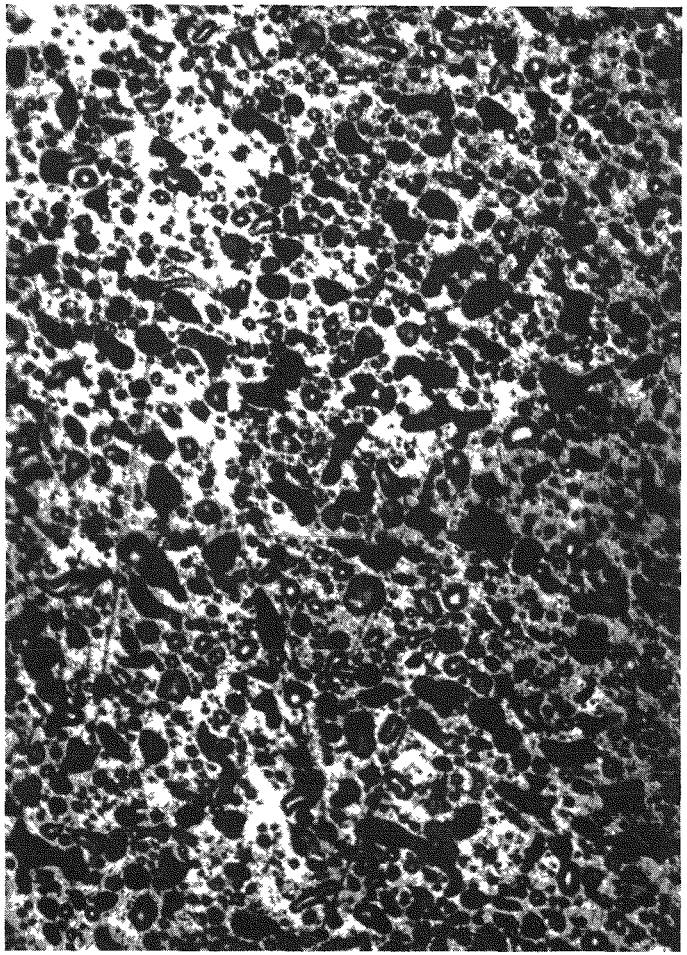

UNAFFECTED FUEL

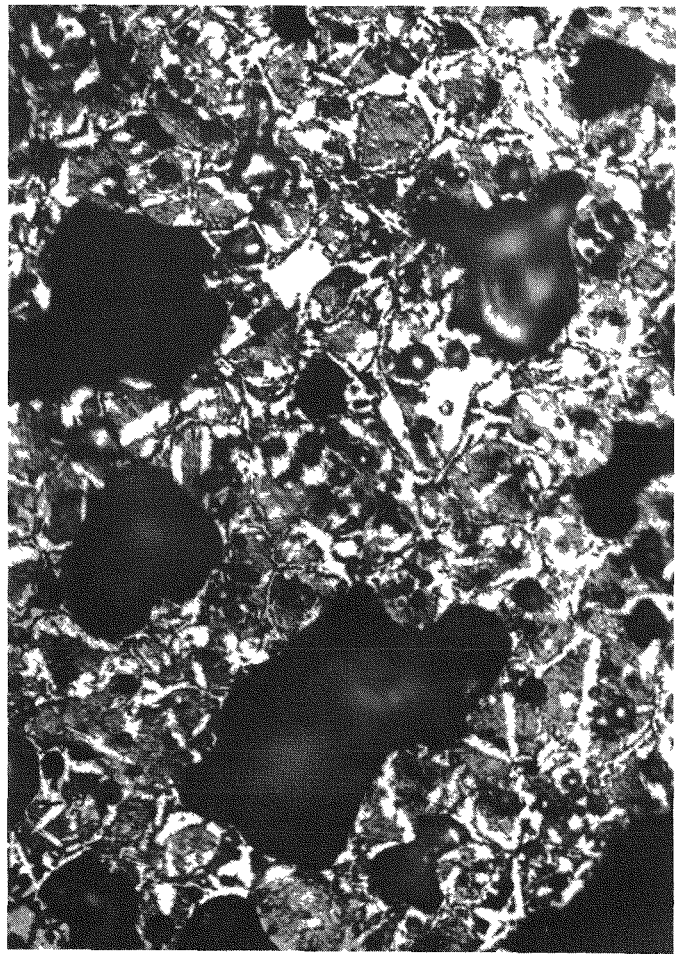

ONCE-MOLTEN FUEL

Fig. 13. Comparison of Microstructure of Reacted and Unreacted Fuel in the 88-02 Test Specimen. (500X, AP, MCT 243998)

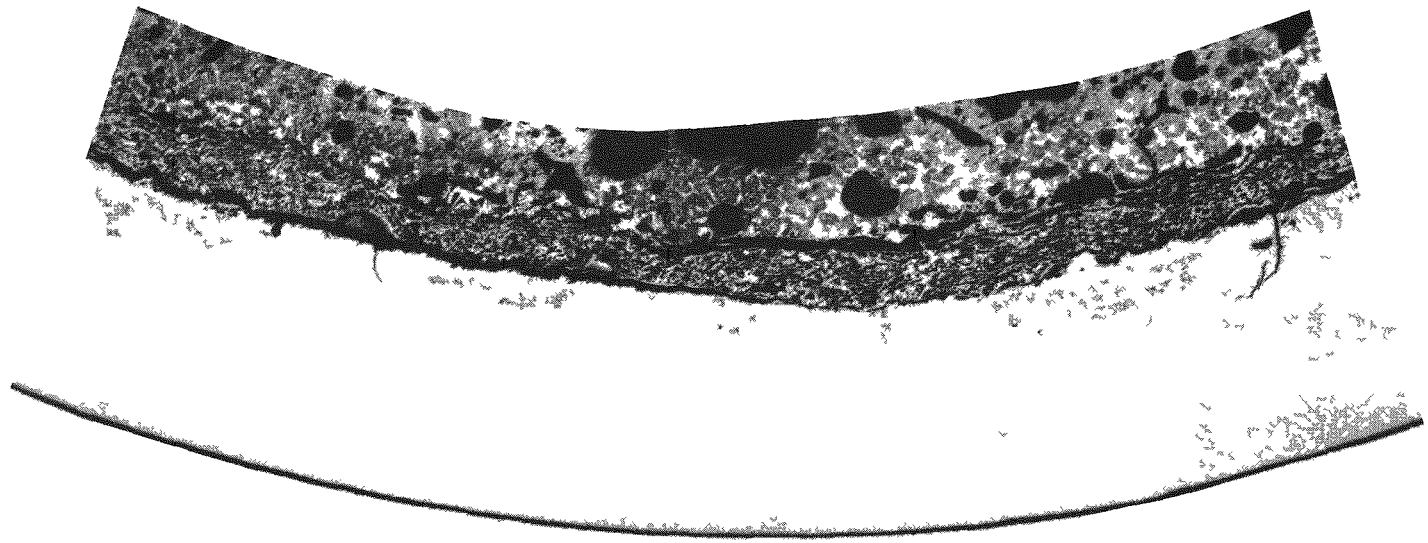

Fig. 14. Condition of the Reacted Fuel and Cladding at the Location Where Maximum Cladding Penetration Occurred in the 88-02 Test Specimen. (83X, AP, MCT 243911)

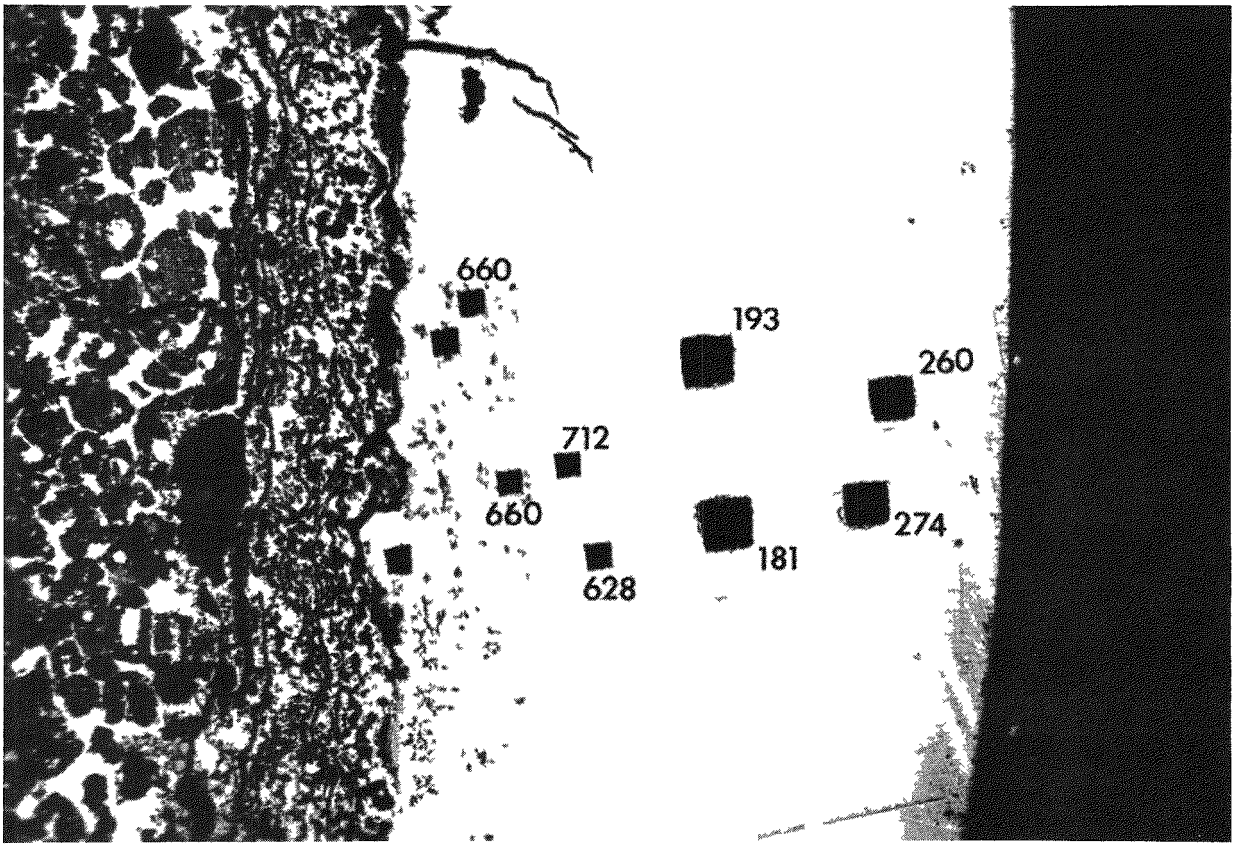

Fig. 15. Results of the Microhardness Measurements Performed on the 88-02 Test Specimen. (200X, AP, MCT 243921)

by SEM, were measured. The results are shown in Table II along with the calculated maximum rate of penetration. For conservatism, the cladding penetration rates from the open-gap specimens were not used in the validation of the existing penetration-rate correlation (see Discussion Section).

C. Results of Scanning Electron Microscopy Examination

From the 800°C, FBTA 88-10 test specimen, two samples, one containing a cladding section and the other containing a fuel section, were prepared for SEM examination. Energy-dispersive X-ray analyses were also conducted on the samples to determine the compositions of the various phases found in the intact and reacted fuel and cladding.

1. Examination of the Cladding Sample

Figure 16 shows the optical image of a section of the prepared cladding sample. The thickness of the reaction zone between the cladding and the fuel was comparable to that observed in the other 800°C test, FBTA 88-04. The cracks in the reaction zone, most likely accentuated during the posttest cutting operations, are indicative of the brittleness of the solidified reaction products. A slight amount of the once-molten fuel adhered to the inside of the reacted cladding zone.

The area that was examined in detail by SEM is outlined in Fig. 16 and shown enlarged in Fig. 17. This area was selected because it contained all of the features found elsewhere in the sample and was relatively free of pores and surface imperfections. Almost all of the SEM/EDX spectral analyses for composition of phases were made in the area outlined in Fig. 17. Enlargements of this area are shown in Figs. 18 and 19, which are the secondary electron (SE) image and the corresponding backscattered electron (BSE) image, respectively. In BSE images, phases with high average atomic number (Z) are light, and phases with low Z are relatively dark.

From Fig. 19, the following phases were identified in the reaction zone: (A) the unreacted cladding, (B) a coarse medium gray phase, (C) a light

TABLE II. Measured and Predicted Penetration Rates

FBTA Test No.	Fuel-Cladding Gap	Test Temp. (°C)	Measured Max. Cladding Penetration (μm)	Measured Max. Penetration Rate (μm/s)	Predicted[a] Max. Penetration Rate (μm/s)
88-06	Closed	700	<3	$<1 \times 10^{-3}$	3.9×10^{-3}
88-05	Closed	750	67	1.9×10^{-2}	1.6×10^{-2}
88-04	Closed	800	164	4.6×10^{-2}	5.5×10^{-2}
88-03	Open	750	<3	$<1 \times 10^{-3}$	1.6×10^{-2}
88-01	Open	800	<3	$<1 \times 10^{-3}$	5.5×10^{-2}
88-02	Open	850	175	4.9×10^{-2}	1.7×10^{-1}

[a]According to the following ANL correlation, with T in K: Penetration Rate (μm/s) = exp[22.847 - (27624/T)].

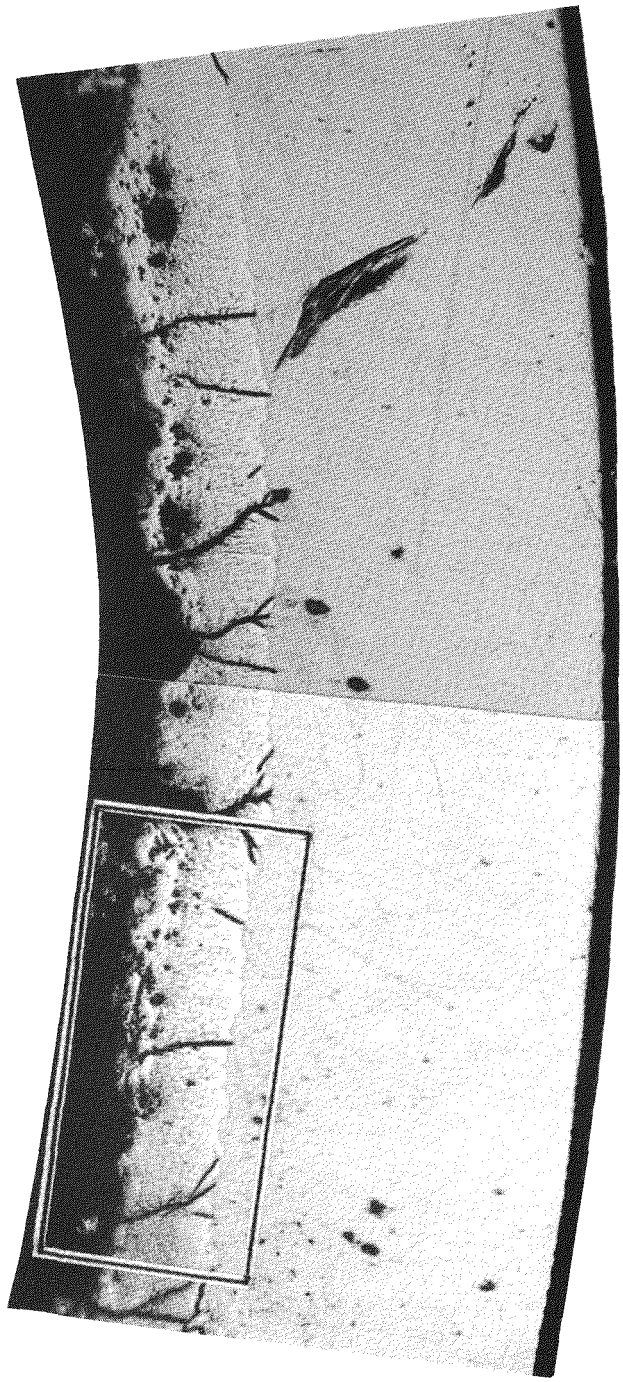

Fig. 16. Optical Image of a Section of the U-10Zr/HT9 Sample Examined with SEM. The specimen was subjected to an 800°C test for 1 hour. (150X, MCT 244286, 244287)

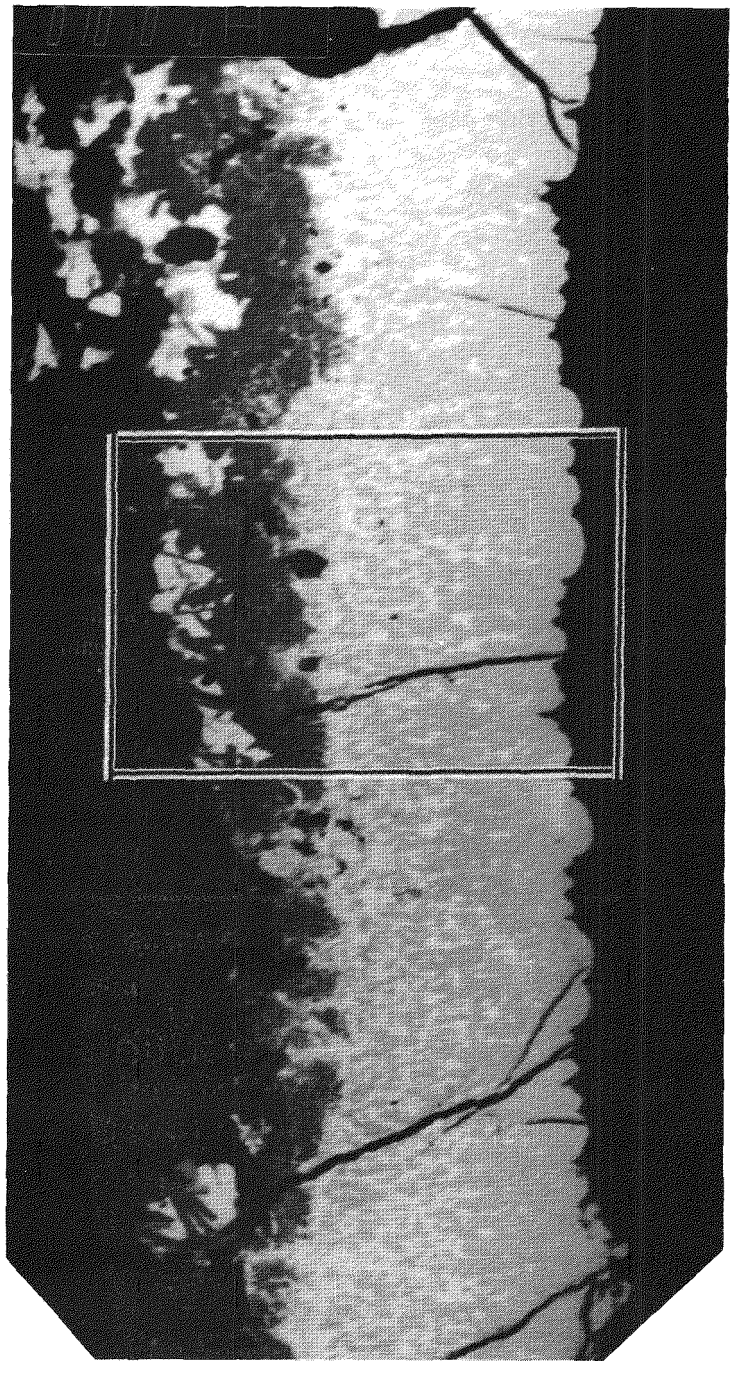

Fig. 17. Backscattered-Electron Image of the U-10Zr/HT9 SEM Sample. Unreacted cladding is the black area to the right. The outlined area is shown at a higher magnification in Figs. 18 and 19. (MCT 308948)

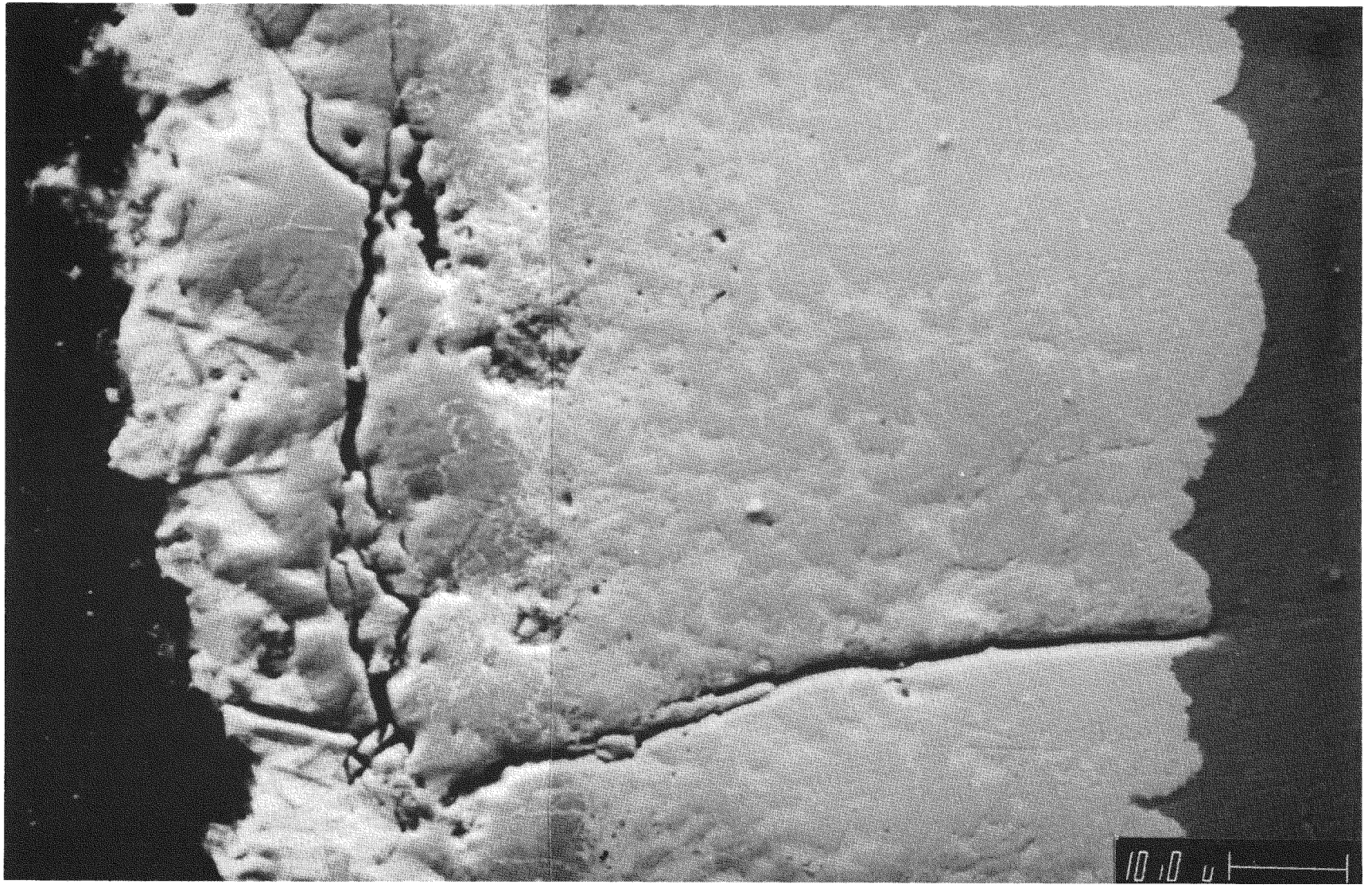

Fig. 18. SE Image of the Outlined Area of Fig. 17. (MCT 308954, 308956)

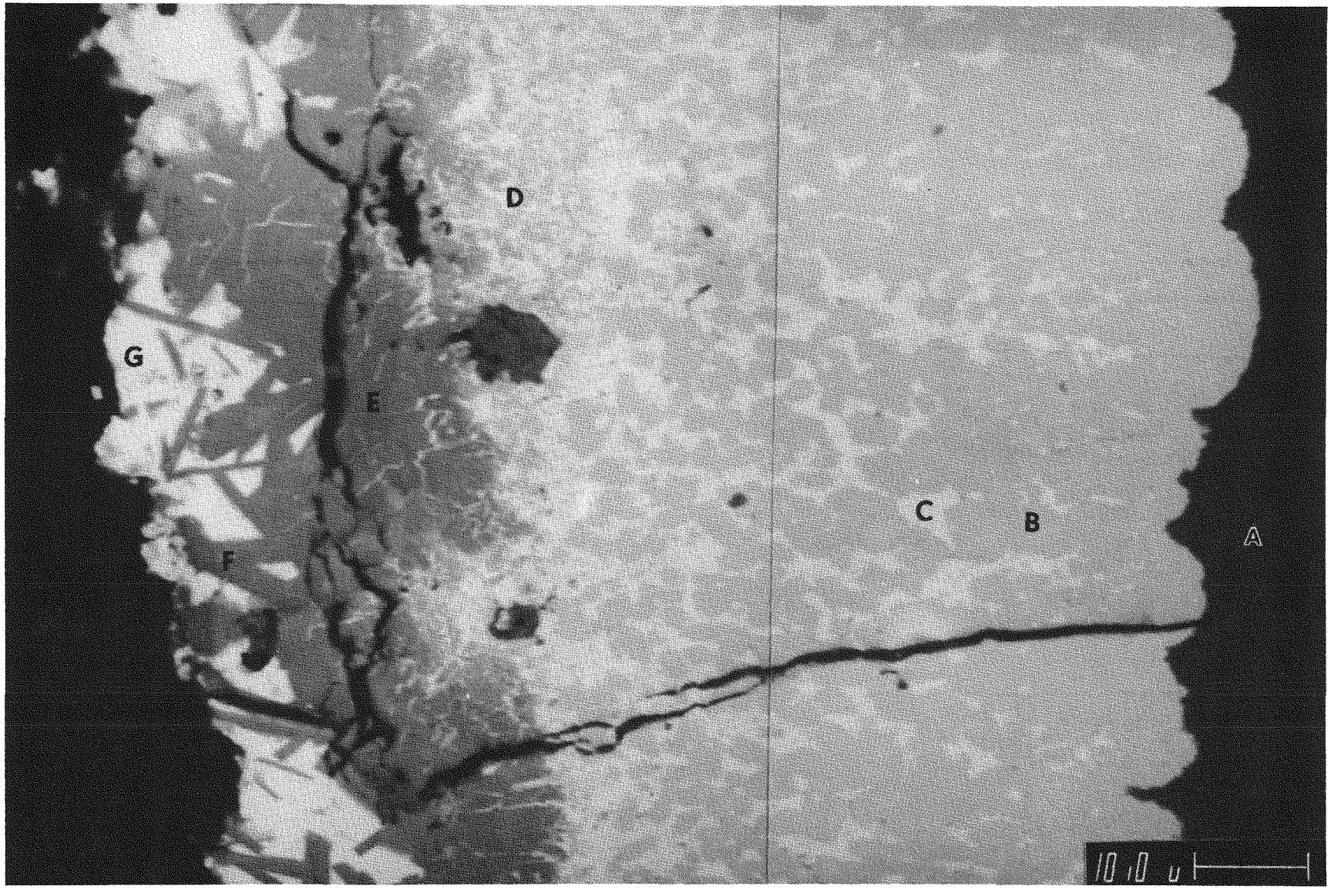

Fig. 19. BSE Image of the Outlined Area of Fig. 17. The various phases (cf. text and Table III) are A) unreacted cladding, B) medium gray phase, C) light gray phase, D) salt-and-pepper structure, E) dark gray phase (band), F) dark gray acicular phase, and G) once-molten fuel. (MCT 308955, 308957)

gray phase, (D) a fine salt-and-pepper structure, (E) a nearly continuous dark gray phase ("band"), (F) a dark gray acicular phase, and (G) the once-molten fuel. The compositions of these zones, from the SEM/EDX analyses, are shown in Table III. The spots and areas where EDX analyses were performed are shown in Fig. 20.

The composition of the unreacted cladding, both immediately adjacent to the well-defined reaction boundary and further away, was essentially that of the original HT9 material. No penetration of U or Zr past the reaction boundary could be detected in the SEM/EDX spectra. The attack on the cladding was a general one by molten fuel-cladding alloy and the resultant reaction boundary had, for the most part, generally rounded fronts into the cladding that met in sharp ridges. No diffusion-controlled sub-phases or intergranular penetration ahead of the visible reaction boundary could be detected on the cladding side of the boundary at magnifications up to ~3000X. The radial crack in the reacted zone terminated exactly at the reaction interface, indicating the unreacted cladding to be ductile and capable of arresting crack propagation. These findings support the assumption, which was used to determine cladding penetration and penetration rates, that there was no further cladding wastage past the visible reaction boundary.

The bulk of the solidified reaction products consisted of a medium gray phase and a light gray phase in a duplex structure. The light gray phase was found in the SEM/EDX analysis to have a composition (67 a/o U, 2.8 a/o Fe, with only a small amount of Cr and Zr) essentially identical with that of the 725°C U-Fe eutectic. The medium gray phase, on the other hand, had a substantially greater Fe content, which ranged from 71 a/o near the reaction boundary to 66 a/o away from the boundary. The high Fe content in the medium gray phase suggests that this phase contains a substantial amount of the intermetallic compound UFe_2. According to the equilibrium diagrams of the major components, the material in this region would have been a solid-liquid mixture with an overall composition on the Fe-rich side of the U-Fe eutectic (66 a/o U, 34 a/o Fe) at the test temperature. During cooldown at the end of the test, additional medium gray UFe_2 phase precipitated by nucleating on the inside wall of the remaining cladding and growing as dendrites into the melt, followed by the solidification of the lower-melting light gray phase.

TABLE III. SEM/EDX Compositions of the Cladding Zones in the FBTA 88-10 Specimen[a]

Zone[b]		U	Zr	Fe	Cr
Cladding adjacent to reaction interface (A)	w/o	T[c]	T	88	12
	a/o	T	T	89	11
Cladding away from interface (A)	w/o	T	T	87	12
	a/o	T	T	88	12
Medium gray phase adjacent to interface (B)	w/o	44	2	46	8
	a/o	16	2	71	11
Medium gray phase away from interface (B)	w/o	44	5	42	8
	a/o	17	5	66	12
Light gray phase (C)	w/o	89	1	9	1
	a/o	67	3	28	2
"Salt-and-pepper" structure (D)	w/o	63	11	23	4
	a/o	31	14	49	7
Dark gray phase (band) (E)	w/o	6	38	40	16
	a/o	2	29	50	19
Dark gray phase (acicular) (F)	w/o	5	44	38	12
	a/o	2	35	49	15
Once-molten fuel (G)	w/o	88	3	9	T
	a/o	67	6	28	1

[a]Compositions given are based on standardless correction technique and averaged from typically three or more readings. The individual readings were quite consistent, except for the Zr contents in the once-molten fuel, which ranged from 0.2 to 6.4 w/o.

[b]Letters refer to types of phases shown in Fig. 19.

[c]Trace quantity.

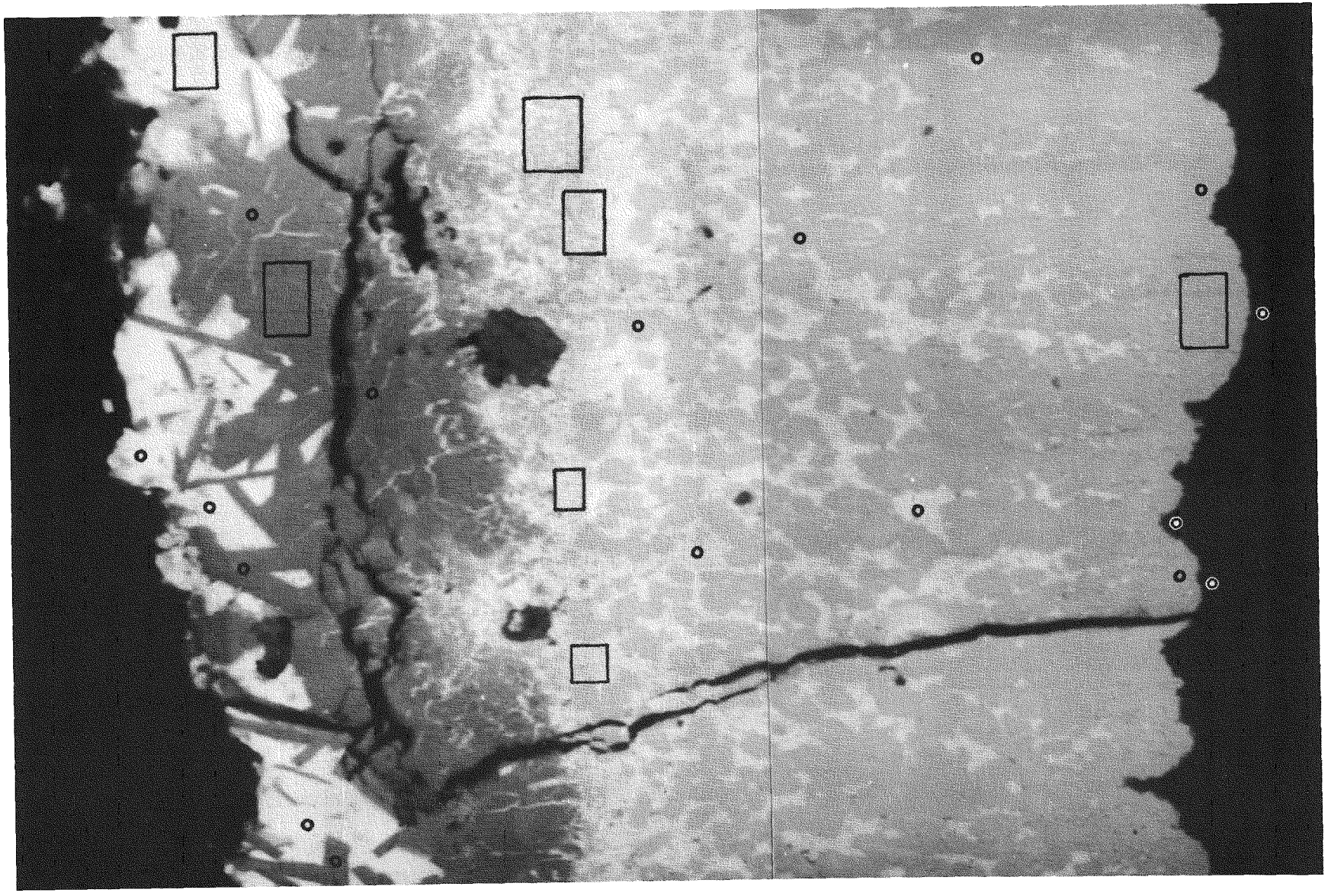

Fig. 20. Locations Where Spot (Represented by Circles) and Areal SEM/EDX Measurements Were Performed. Four additional measurements were made but not shown in this figure: two areal measurements on cladding away from the reaction interface, one spot measurement on the dark gray phase, and another spot measurement on the once-molten fuel.

The adjacent "band" and acicular areas in Fig. 19 had similar dark gray appearances and were found to have nearly identical compositions in the SEM/EDX spectral analyses, Table III. They contained essentially Zr, Fe, and Cr, with only a minor amount of U (<2 a/o). The measured atomic compositions of 29-35 a/o Zr and 63-69 a/o Fe+Cr in these components strongly suggests that they are related to the $ZrFe_2$ and $ZrCr_2$ compounds. Much of the Zr in the nearly continuous band was probably from the high-Zr layer on the fuel surface. The aciculas were then formed by crystalline growth inward at the expense of the molten fuel phases. Both the $ZrFe_2$ and $ZrCr_2$ compounds are known to be very stable in the U/Zr/Fe+Cr system and their formation is thermodynamically favored over uranium intermetallics. The higher Cr:Fe ratio in these dark gray phases, vis-a-vis the original Cr:Fe ratio in HT9, suggests that Zr has a greater affinity for Cr than for Fe.

The small size of the particles in the salt-and-pepper material precluded their individual SEM/EDX analysis. At higher magnification, there appear to be small particles representative of the shades in both the medium gray phases to the right and the dark gray phases to the left. Spectra of four representative salt-and-pepper areas were averaged to get the overall composition of the salt-and-pepper material in Table III.

As is evident in Figs. 17 and 19, only a small amount of the once-molten fuel phase adhered to the cladding segment. The composition of this phase was mostly U and Fe, in an atom ratio very close to the 725°C U-Fe eutectic composition. The Zr content in this phase was low and not uniform (ranging from 0.4 to 12 a/o at various spots). The Cr content, particularly with respect to the Fe content in the original HT9 material, was also low (<1 a/o). The depleted Zr and Cr contents in this phase were consistent with the fact that a high concentration of Zr and Cr was found in the adjacent dark gray phases.

2. Examination of the Fuel Specimen

The fuel sample examined by SEM was a very small piece from the outer region of the fuel. Because of the difficulties in preparing and mounting the tiny specimen, it was not possible to determine how close it was to the

cladding interface or whether the specimen was mounted truly transversely. Two elevations of this fuel sample were examined. The first elevation (Surface A) showed only the reacted fuel. After the examination was completed on Surface A, the specimen was subjected to additional grinding and polishing to produce the second elevation (Surface B), in which the transition zone between the reacted fuel and the inner unreacted fuel was revealed.

a. Surface A

Surface A contained reacted fuel exclusively. With its apparently high density and large, spherical pores, its morphology is typical of that of once-molten fuel materials. The SE images of Surface A is shown in Fig. 21. The outlined box in Fig. 21 denotes the area examined in detail by SEM. Higher magnification SE and BSE images of this area are shown in Fig. 22.

The BSE image of Surface A shows that the once-molten fuel consists primarily of two phases: a dark gray acicular phase and a light gray matrix phase. (The duplex nature of this structure is similar to the one shown in Fig. 13.) Some of the dark gray acicular particles have a somewhat rounded cross section, but in terms of composition, they are the same as the straight-edged acicular particles. In the SEM/EDX spectral analyses, the acicular particles were found to have a composition of ~44 a/o Zr, ~44 a/o Fe, and balance U. This composition suggests that the acicular particles consist of a mixture of the Fe_2Zr and $FeZr_2$ compounds and are related to the dark gray phases found in Fig. 19 at the fuel-cladding interface. Because of the high melting points of the Zr-Fe compounds (>1000°C), the acicular particles are believed to have formed during the one-hour 800°C test and were not the result of solidification during the cooldown. The formation of the solid acicular particles in the liquid apparently caused the cellular-appearing structure, where the dark particles seem to be outlining specific small areas of the matrix. This is particularly evident near the surface (at the right side of Fig. 22), where the particles are rather small and perhaps represent an early manifestation of the larger, inward particles. This size distribution is probably related to the local availability of Zr, which was likely low in the

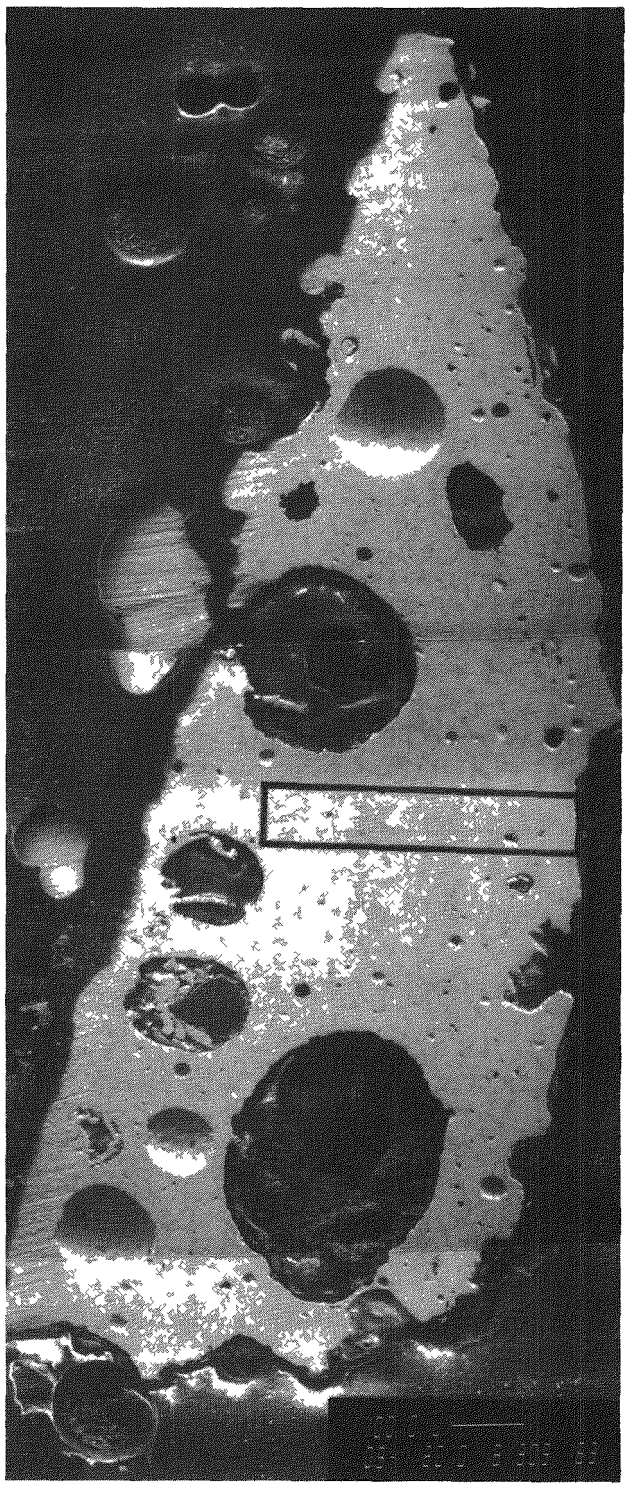

Fig. 21. SEM Image of the Once-Molten Fuel of Surface A. The cladding side is to the right. The outlined area was examined in detail by SEM and is shown at a higher magnification in Fig. 22.

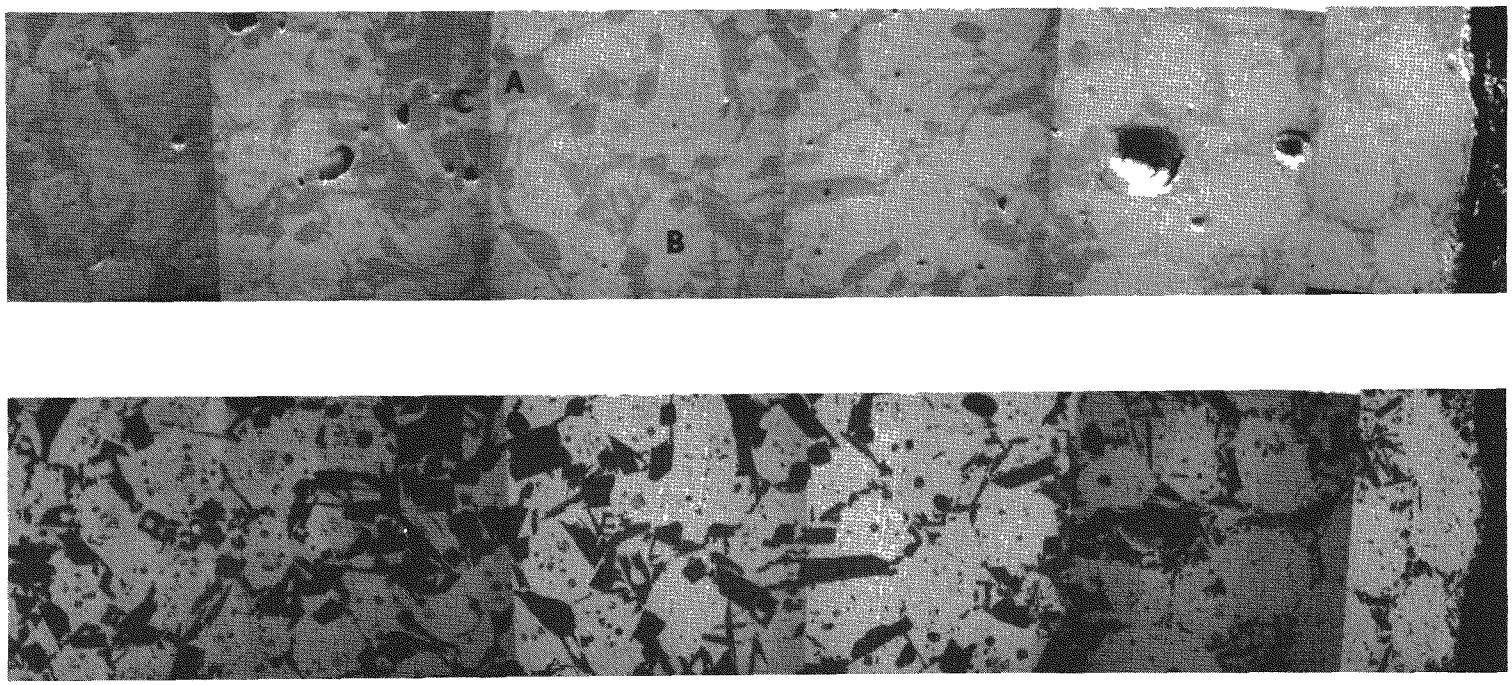

Fig. 22. SE (Top) and BSE Images of the Outlined Area of Fig. 21. The principal phases are acicular particles (A) and fuel matrix (B). There are also a few high-Zr globules (C). (~320X, MCT 309165-30917)

fuel immediately adjacent to the surface owing to the formation of the Zr-rich surface layer.

The light gray matrix phase was found to be the U fuel with a depleted Zr content (~11 a/o or 5 w/o vs. the nominal 10 w/o as-built composition). The depleted Zr content is consistent with the presence of the high-Zr acicular particles in the duplex structure. The Fe content in the matrix phase was low (<~5 a/o) and near the limit of SEM/EDX resolution. (In order to have liquid-phase formation at 800°C, however, only ~1-2 a/o of Fe is required in the U matrix.)

A few dark gray globules were found in the midsection of the area and examined. These globules were probably the carbon- and/or oxygen-stabilized Zr particles that have been shown to be highly stable during irradiation and out-of-reactor testing.

The SEM/EDX compositions of the phases found in Surface A are summarized in Table IV.

b. Surface B

Surface B, shown in Fig. 23, contains the transition zone from the once-molten region to the unreacted region. The once-molten reacted fuel has the same appearance as noted in Surface A (i.e., with a highly dense duplex structure and a few large pores), whereas the unreacted fuel essentially retains the as-irradiated microstructure characterized by numerous, but much smaller, fission gas bubbles.

The transition from the reacted and unreacted fuel is shown at a higher magnification in Fig. 24. Some liquid phase formation was found to have occurred in the transition zone. The transition zone was rather narrow, with a width of only ~50 μm. Immediately on the molten side of the transition zone, the incipient formation of small acicular particles can be noted. Away from the melt boundary, the acicular particles grow substantially larger in size. The compositions of these small and large acicular particles were

TABLE IV. SEM/EDX Composition of the Fuel in the 88-10 Specimen at Surface A[a]

Phase		U	Zr	Fe	Cr
Medium gray acicular particles (with straight edges)	w/o	33	41	25	Trace
	a/o	13	43	44	Trace
Medium gray acicular particles (with rounded edges)	w/o	29	43	27	Trace
	a/o	12	44	45	Trace
Light gray matrix	w/o	93	5	1	Trace
	a/o	84	11	5	Trace
Dark gray globules	w/o	17	80	3	Trace
	a/o	7	88	5	Trace

[a]Compositions given are based on standardless correction technique and are averages of, typically, three or more readings.

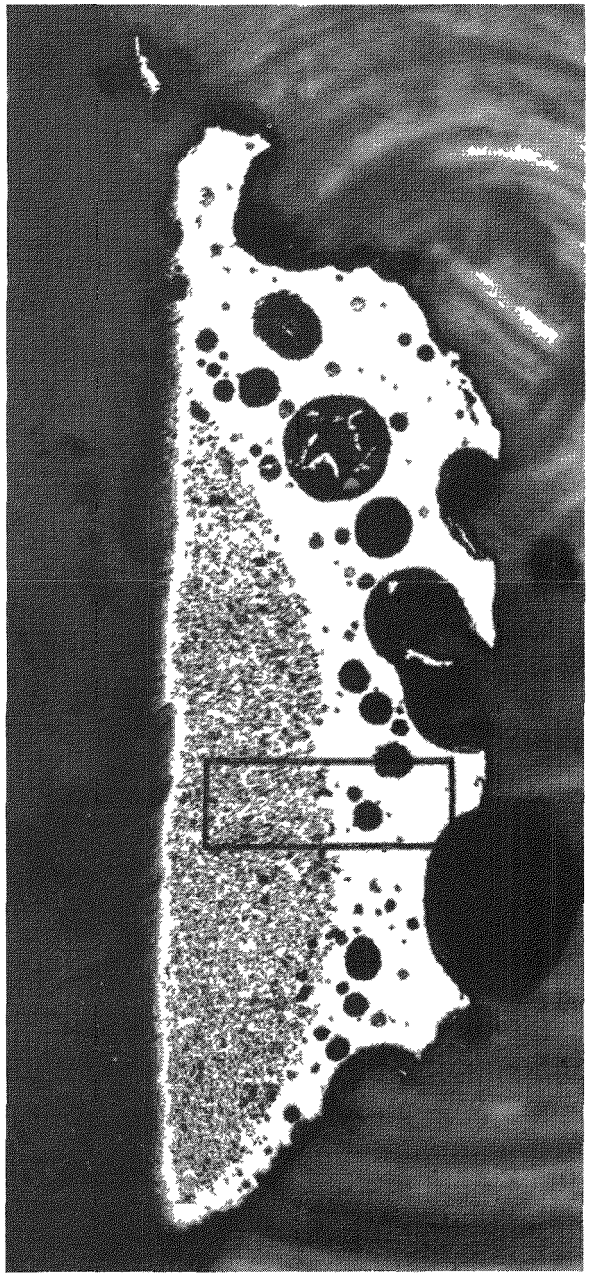

Fig. 23. Optical Photograph (50X) of Surface B. The porous fuel on the left side of the specimen was unreacted. Cladding was to the right. The outlined area is shown at a higher magnification in Fig. 24.

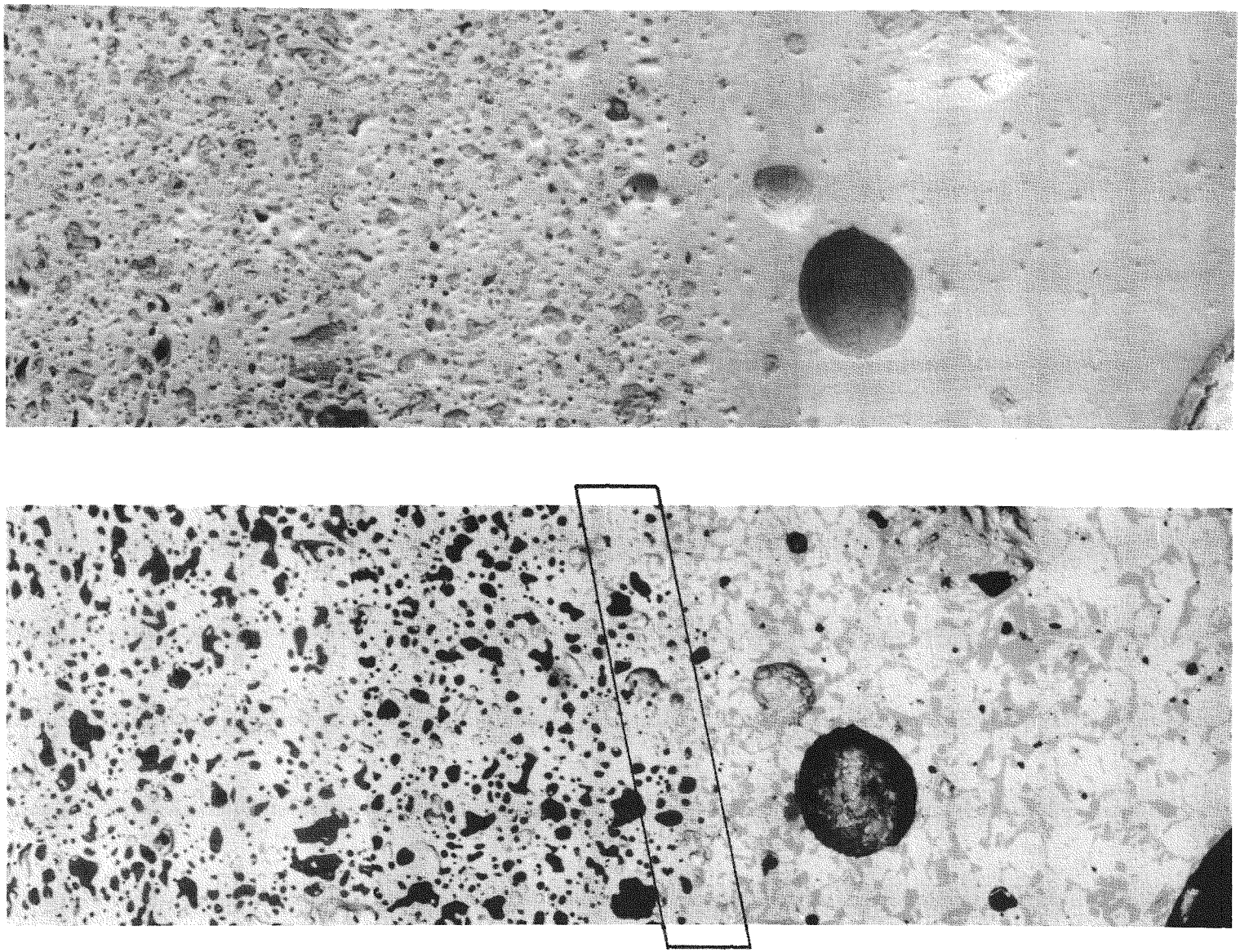

Fig. 24. SE (Top) and BSE Images of the Outlined Area of Fig. 23. The marked area denotes approximately the transition zone between the once-molten fuel (right) and the unreacted fuel (left). (260X, MCT 245033)

essentially the same: ~45 a/o Zr, 43 a/o Fe, balance U. This composition was consistent with that of the acicular particles analyzed in Surface A.

The composition of the unreacted fuel, both adjacent to and away from the melt boundary, was found in the EDX analyses to be ~71 a/o U and ~29 a/o (13 w/o) Zr, with no traces of Fe. The composition of the matrix phase in the once-molten zone, similar to that on Surface A, was depleted in Zr (~10 a/o) and showed only a minor concentration of Fe (<~5 a/o). The SEM/EDX compositions of the phases found in Surface B are listed in Table V.

The interior surfaces of the large pores in the once-molten zone were lined with numerous acicular particles. One such pore is shown in Fig. 25. The orientation of these acicular particles lining the free surfaces was essentially random; however, a distinct 60° orientation relationship can be seen between some of the needles. The pore appears to be a shrinkage void from which molten material has moved, leaving the solid needles.

V. DISCUSSION

A. Onset of Fuel-Cladding Interaction

The test results showed that the onset of fuel-cladding interaction in the U-10Zr/HT9 fuel system, resulting in the formation of liquid phases, occurred between 700 and 750°C, possibly nearer the 725°C eutectic temperature of the U-Fe binary system. These results are therefore not in agreement with the earlier test data, which showed that the eutectic temperature would increase to ~835°C when >~10 w/o of Zr was added to the U fuel.[4] It is possible that the higher eutectic temperature in the earlier tests was caused by a greater interstitial content in the fuel and cladding.[5] A higher interstitial content would promote the formation of the high-Zr surface layer, thereby retarding the fuel-cladding interaction. The lower eutectic formation temperature in the current tests may be explained by noting the nature of the Zr-rich layer and the phases that existed in the fuel-cladding interface. In the current tests, owing to the lower interstitial contents in the fuel and cladding, formation of a Zr-rich layer on the fuel surface in situ during

TABLE V. SEM/EDX Composition of the Fuel in the 88-10 Specimen at Surface B[a]

Phase		U	Zr	Fe	Cr
		In the Once-Molten Fuel Zone			
Medium gray acicular particles	w/o	32	43	25	Trace
	a/o	13	45	43	Trace
Light gray matrix	w/o	93	5	1	Trace
	a/o	84	11	5	Trace
		In the Unreacted Fuel Zone			
Unreacted fuel matrix	w/o	86	13	Trace	Trace
	a/o	71	29	Trace	Trace

[a]Compositions given are based on standardless correction technique and are averages of, typically, three or more readings.

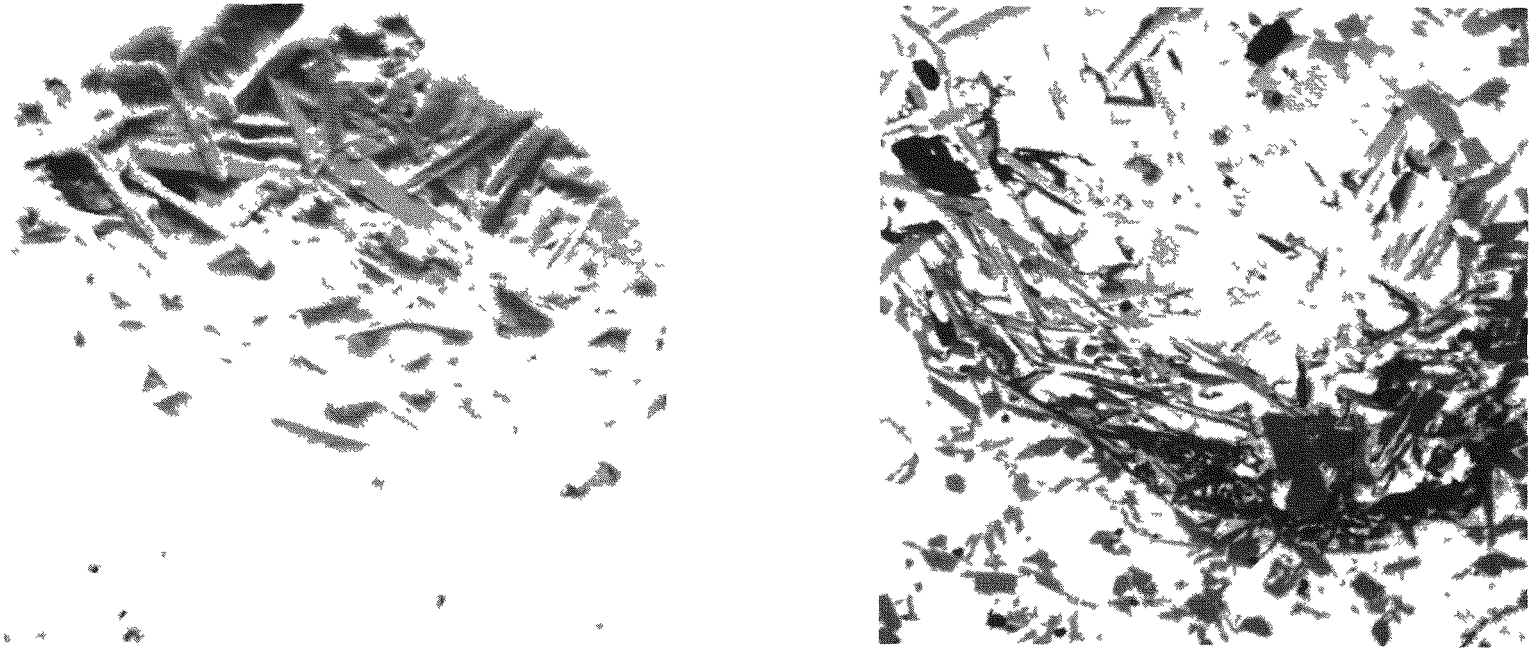

Fig. 25. SE (Left) and BSE Images of the Interior Surface of a Bubble in the Once-Molten Fuel. (500X, MCT 309396, 309397)

irradiation is probably not significant. The Zr-rich layer found on the fuel surface of the current tests, instead, would most likely be the result of the fuel slug casting process. As the layer cracked during irradiation because of the swelling of fuel underneath, direct contact of cladding with fuel then became possible. At the irradiation temperatures, the fuel surface probably consisted of a mixture of alpha- and delta-U phases. Whereas the solubility of Zr in the delta-U phase is high, that in the alpha-U phase is rather low (<1 w/o). Thus, when the alpha-U phase is in direct contact with the Fe-based HT9 cladding, it is conceivable that they would react in a manner similar to that in the binary U-Fe system, i.e., in the absence of Zr.

The observed reaction kinetics appeared to be strongly affected by the condition of the fuel-cladding interface. Less interaction was noted in test specimens from the top end of the fuel column where the gap closure was not complete. Since the top end of the fuel pins will usually experience a higher temperature during a reactor accident, particularly a transient overpower event, the open fuel-cladding gap will likely mitigate the fuel-cladding interaction, at least in the lower-burnup pins.

The test data showed that the Zr-rich layer on the fuel surface could significantly retard fuel-cladding interaction. It may, therefore, be possible to employ one of the following approaches to further enhance fuel-cladding compatibility: (1) introducing interstitials to the fuel or bond sodium to promote the formation of the surface layer or (2) incorporating a protective barrier on the cladding inner surface.

B. Depth and Rate of Cladding Penetration

The reaction boundary in the cladding in the tests was found to be well-defined with no indications of intergranular penetration into the cladding. Whereas the reaction products were brittle at room temperature, the intact cladding was ductile and capable of arresting crack propagation. Without intergranular penetration, no premature cladding failure due to stress concentration would likely occur in-reactor.

When the calculated penetration rate data (Table II) are plotted against the current ANL correlation, Fig. 26, which was derived on the basis of past tests (dipping, furnace, DEH, etc.) on various fuel-cladding systems (U/Fe, U-Fs/304 SS, U-Pu-Zr/HT9, etc.), the agreement was found to be very good. The ANL correlation, in the temperature range between 725 and 1000°C, can be described by the following Arrhenius equation:

$$S = \exp[22.847 - (27624/T)]$$

where S = penetration rate (in micrometers per second) and T = cladding inner-surface temperature (in K).

The current FBTA test data provide additional validation, particularly in the lower temperature range, for the ANL correlation. (As stated before, the penetration rates from the open-gap specimens were excluded owing to their less conservative nature.)

C. Role of Zr in the Fuel-Cladding Interaction

The SEM/EDX examination results showed that (1) Fe was always present in the reacted fuel and (2) no Fe was present in the unreacted fuel. Furthermore, the data showed that Fe reacted preferentially with Zr in the fuel matrix and formed stable Zr/Fe compounds. When this occurred, the Fe content in the fuel matrix was effectively reduced. By acting as a "sacrificial" material, the Zr in the fuel matrix, or on the fuel surface, might have slowed down the Fe penetration into the fuel.

VI. CONCLUSIONS

1. The fuel-cladding interaction between U-10Zr and HT9 cladding was found to be a liquid-alloy attack of the cladding. Onset of reaction occurred between 700 and 750°C.
2. Liquefaction of the fuel was due to the infusion of Fe from the cladding. The unreacted fuel contained no Fe.

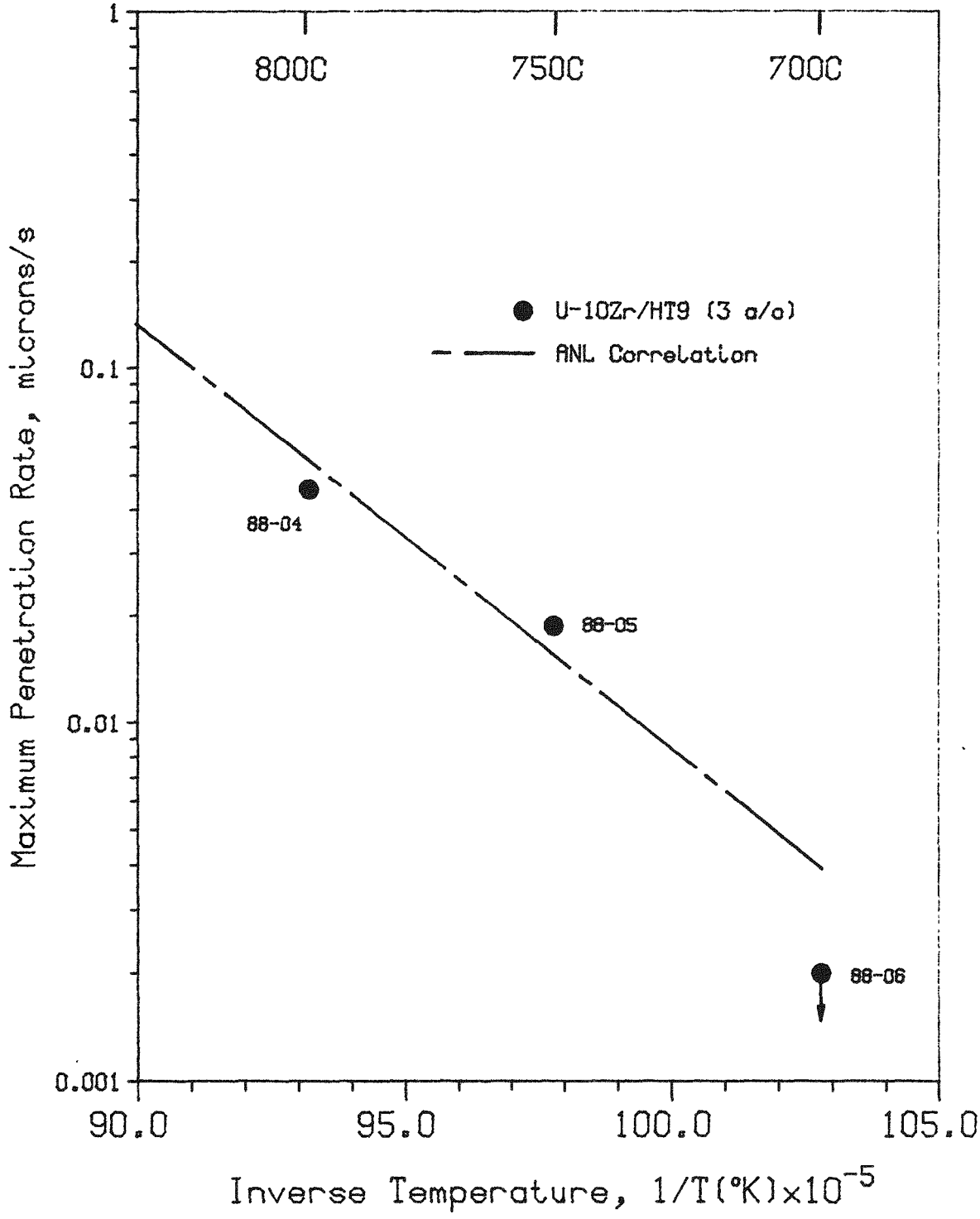

Fig. 26. Comparison of the Measured Maximum Cladding Penetration Rate with the ANL Correlation.

3. The reaction kinetics are strongly affected by the condition of the fuel-cladding interface. The presence of a Zr-rich layer on the fuel surface can significantly retard the cladding penetration.

4. Likewise, the reaction kinetics are greatly retarded if the gap between the fuel and cladding is not fully closed.

5. The measured cladding penetration rates conform well to the existing ANL correlation.

6. The Fe that was removed from the cladding was found to react preferentially with the Zr in the fuel and to form stable Fe/Zr phases. This resulted in a lowered Fe content in the U matrix and possibly slowed down the Fe penetration into the fuel.

VII. ACKNOWLEDGMENTS

The authors wish to thank W. N. Beck for making the irradiated fuel specimens available for testing; H. Lautermilch, C. Gebo, and W. Kremsner for characterizing the specimens before and after the tests; L. A. Neimark for many valuable insights and helpful discussions; and C. A. Bertino for preparation of the report.

VIII. REFERENCES

1. Pahl, R. G., et al., "Postirradiation Examination of the HT9 Clad Fuel Test at 2.9% Burnup," ANL-IFR-81, November 1987.

2. Fenske, G. R., et al., "Direct Electric Heating of Irradiated EBR-II Mark-III Driver Fuel," ANL-IFR-17, June 1985.

3. Fenske, G. R., et al., "Fission Gas Retention and Axial Expansion of Irradiated Metallic Fuel," ANL-IFR-45, June 1986.

4. Zegler, S. T., and Walte, C. M., "Compatibility Between Metallic U-Pu-Base Fuels and Potential Cladding Materials," AIME Symposium on Nuclear Fuels Technology, Nuclear Metallurgy 13, 335-344, October 1967.

5. Kelman, L. R., Argonne National Laboratory, private communication, 1986.